Full Length Article

Flare gas-to-power by direct intercooled oxy-combustion supercritical CO_2 power cycles

Ahmad K. Sleiti, Wahib A. Al-Ammari [*], Khaled M. Aboueata

Department of Mechanical & Industrial Engineering, College of Engineering, Qatar University, Doha, Qatar

A B S T R A C T

With more than 150 billion m^3 of gases annually flared around the world, gas flaring is a major source of greenhouse gas emissions that contaminates the environment with more than 400 Mt CO_2/year. Therefore, utilizing the flared gases efficiently becomes inescapable and one of the most promising utilization technologies is using Gas-to-Power (GTP). However, most of the available GTP technologies are still using conventional power cycles that have limited efficiencies and produce high-level of emissions. Herein, we use direct oxy-combustion (DOC) supercritical CO_2 (sCO_2) power cycle, instead, to realize the desired no flaring-no emissions solution. Two innovative flared-intercooled sCO_2 power cycles that utilize flare gases and natural gas as fuel are introduced. In the first flared power cycle (FPC1), the flare gases are mixed with the natural gas before being combusted in the DOC. While in the second cycle (FPC2), the flare gases are used to perform a reheating process for the exhaust flow of the primary heater (DOC) after being partially expanded in a high-pressure turbine. Comprehensive energetic, exergetic, exergoeconomic, levelized cost of electricity (LCOE), and multi-objective optimization analyses are conducted for each configuration over practical ranges of operating conditions for six flare gas samples that significantly differ in their composition and specifications. A minimum LCOE of 5.02¢/kWh is achieved by sweet flare gas sample in FPC1 at T_{max} of 731 °C, P_{max} of 300 bar, P_{min} of 40 bar, T_{min} of 32 °C, and $\dot{W}_{net}$ of 50 MW with energy efficiency of 45.10%. At the optimized conditions, FPC1 and FPC2 show superior energetic and economic performances compared to indirect-combustion power cycles, however, indirect combustion of flare gases may perform better than FPC2 at low capacities and therefore recommended for future work.

1. Introduction

In oil & gas, and petrochemical industries, flaring of excess gas (the process of burning-off associated gas from wells, hydrocarbon processing plants, or refineries) is a standard process to release the gas for safety and pressure control. According to the World Bank reports, around 140 to 150 billion m^3 of gases are annually flared around the world (See Fig. 1), which is equivalent to the annual gas consumption of Sub-Saharan Africa [1–3]. Consequently, gas flaring is considered as a major source of greenhouse gas emissions that contaminates the environment with about 400 Mt CO_2 per year [4,5]. Concurrently, the composition of the flared gases is very similar to natural gas (NG), which is a cleaner source of energy than other fossil fuels. In view of the increasing gas prices since 2005 alongside the growing concerns about the depletion of oil & gas resources [6], environmental effects, and the economic losses associated with gas flaring, flare gas recovery technologies must be considered as an imperative solution to mitigate these

issues. One of the most promising technologies is using Gas-to-Power (GTP) conversion. For instance, around 60 billion kWh of power can be generated from the annually flared gas in Iran [7]. This amount of power forms almost 30% of Iran's annual power consumption and could save 5 billion dollars annually. Similarly, around 4.6 billion kWh can be generated from the annually flared gas in Qatar (1.11 billion m^3/year), which is about 12% of its annual power consumption (37.24 billion kWh/year). However, most of the available GTP technologies are still using conventional power cycles that have limited efficiencies and produce high-level of emissions. Using direct oxy-combustion (DOC) supercritical CO_2 (sCO_2) power cycle, instead, provides the desired no flaring-no emissions solution, which is the focus of the present study. Next, the available flare gas recovery technologies are reviewed and compared in subsection 1.1 focusing on flare GTP in subsection 1.2 and on the potential of utilizing flare gas in DOC sCO_2 power cycles in subsection 1.3.

Nomenclature

Symbols

A	heat transfer area, (m^2)
$\dot{E}$	exergy rate, (kW)
f	temperature correction factor of the cost correlations
h	specific enthalpy, (kJ/kg)
$\dot{m}$	mass flow rate, (kg/s)
$\dot{n}$	molar flow rate, (kmol/s)
n	lifetime of the plant, (years)
P	pressure, (bar)
$\dot{Q}$	heat transfer rate, (kW)
R	gas constant, (kJ/kg-K)
T	temperature, (°C & K)
U	overall heat transfer coefficient, (kW/m^2-°C)
$\dot{W}$	power produced or consumed by a layout component, (kW)
x_j	molar fraction
Z	component cost, ($, in 2019)
η	energy, mechanical, or isentropic efficiency, (%)
ε	exergy efficiency, (%)

Subscripts

1, 2, 3, …	state points as shown in Fig. 2 and Fig. 3
ch	chemical
CO_2	produced carbon dioxide at the outlet of the combustor
DTS	depreciation tax shield
$flare$	flare gas
F,k	fuel exergy of component k
g	Generator
i	Inlet
LOC	lifetime operating costs
L,k	loss exergy
max	maximum

min	minimum
NG	natural gas (methane)
net	net output
o	outlet (also ambient)
overall	for the overall exergy efficiency of the cycle
P,k	product exergy
ph	physical
rCO_2	recycled carbon dioxide to the combustor
th	for the thermal efficiency of the cycle

Acronyms

ASU	air separation unit
DP	depreciation period
DR	discount rate
FC	fuel compressor
GC	gas compressor
GT	gas turbine
GTP	Gas-to-Power
HTR	high temperature recuperator
IC	intercooler
LCOE	levelized cost of electricity
LEP	lifetime electrical production
LHV	lower heating value
LTR	low temperature recuperator
MOF	Multi-objective function
OC	oxygen compressor
OMC	operating and maintenance cost
PUF	plant utilization factor
PV	present value
SOF	Single objective function
sCO2	supercritical carbon dioxide
TR	tax rate
PC	precooler
WS	water separator

1.1. Flare gas recovery and utilization technologies

Several technologies have the potential to be used for the recovery and utilization of the flare gas as presented in Table 1. The application of these technologies for flare gas recovery depends on several decision drivers such as the gas composition, capital & operating costs, process location (onshore/offshore), safety considerations, technology maturity, production profile, revenue, transportation to market, and community interdependency. However, the fluctuation of the flow rate and composition of the flare (especially from downstream sources such as refineries and petrochemical plants) makes most of these technologies not applicable for flare recovery. Furthermore, the high flow rate and
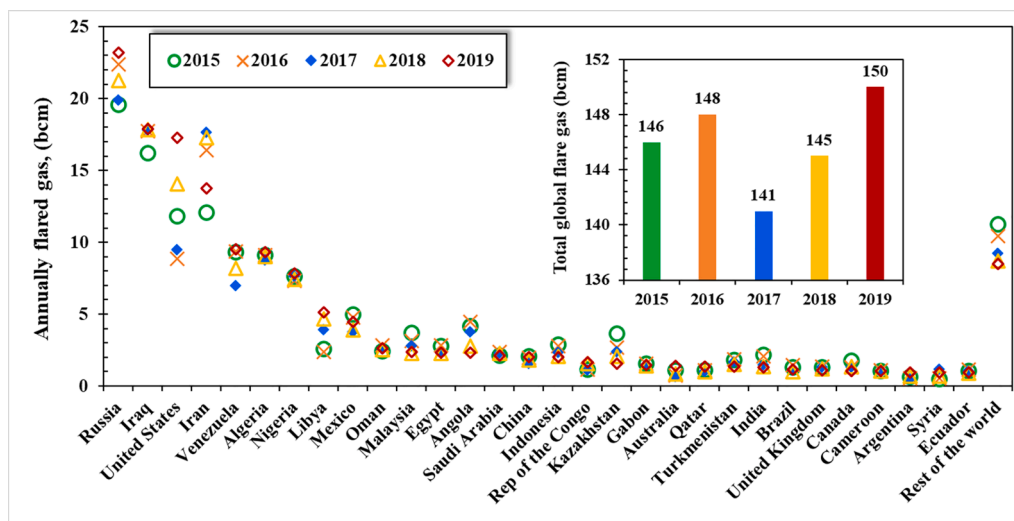

Fig. 1. Annually flared gas around the world from 2015 to 2019 (billion cubic meters (bcm)).

Table 1
Technologies considered for flare gas recovery and utilization [7,10–16].

Technology	Market/ application	Features	Concerns and limiting factors
Process feed or fuel gas	- Refineries - Power generation	- Reduced visible flame - Reduced sound	- Composition of flare gas - High compression cost
Gas pipelines	- Domestic gas grid - Power plants - LNG & GTL plants	- Has the lowest cost in case of short distances and large market	- Land ownership-Fluid phase behavior-Transportation distance
Gas reinjection	- Enhanced oil recovery - Clearance of highly contaminated gases	- Reinjection costs are less than of Sulfur removal process	- Reservoir engineering considerations - High compression cost
Natural gas liquids (NGL)	- NGL plants		- High Capital and operational costs
Liquified natural gas (LNG)	- Fuel in power stations - LPG	- More safe and cheap for long-distance markets - High storage capability	- Road safety
Compressed natural gas (CNG)	- Fuel for industries and power generation	- Short & medium distances - Much simpler and less costly than LNG	- Lower capacity than LNG - High risk of explosion
Natural gas hydrates (NGH)	- Fuel for industries and power generation	- More economical for gas transportation	- Still in laboratory-scale - Lower capacity than LNG
Gas to liquid (GTL)/ Gas to chemicals (GTC)	- Hydrogen production - Methanol production - Ammonia production	- Suitable for large distance transportation - Cleaner than tradition. fuels	- Require high flow rate and specific composition - Lack of maturity
Gas to power/ gas to wire	- Generate electricity	- Minimal gas pretreatment - Less sensitive to variable flow rate and composition	- Capital and operational cost need consideration

methane content required for the NGL and gas pipeline processes make them suitable only for the associated gases (which are found with deposits of petroleum). On the other hand, gas-to-power technologies are more flexible and less sensitive to the flow rate and composition fluctuations [7]. Therefore, the gas to power technologies are more suitable for flare gas recovery for both upstream and downstream sources [8,9]. However, this option has not been considered in operational or planned projects.

1.2. Power generation using flare gas

Only few studies have been conducted on the utilization of the flare as fuel for electricity generation with a focus on the environmental, economic, and political impacts such as those presented in [17–21]. In particular, Heydari et al. [14] investigated two scenarios for reusing the flare gas including power generation and adding the Fog method to improve the efficiency of the gas turbine. The second scenario extracts more power than the first one; however, the first scenario is more economically justified. Also, Heidari et al. [22] developed two feasible configurations to recover flare gases to drive a combined gas power cycle either by mixing the flare gas with conventional fuel in the combustion chamber (configuration 1) or by using flare gas to perform reheating process (configuration 2). From technical and economical point of views, they concluded that configuration 1 is preferable with

the variable flow rate of the flare. However, configuration 2 has superior performance at a flare flow rate less than 0.8 kg/s. Recently, Nezhadfard and Khalili-Garakani [7,23] investigated four power generation configurations for flare gas recovery including (i) gas turbine cycle, (ii) combined gas turbine cycle, (iii) reciprocating internal combustion engine (RICE), and (iv) solid oxide Fuel Cell/gas turbine (SOFC/GT) cycle. They investigated the economic and environmental performances of these configurations using 8 different flare gas samples from different sources. According to the results, the RICE and SOFC/GT cycles have the best and worst economic performance, respectively.

While the proposed configurations in the aforementioned studies are capable to reuse flare gases to generate power, the combustion products (mainly CO_2) are eventually discharged into the atmospheric air, which is one of the major concerns of the conventional flaring process. In other words, these configurations make economic benefits by flare recovery to generate power; however, they have not solved the environmental issues of the flaring process. To recover the flare gases without any CO_2 emissions, a DOC sCO_2) power cycle should be used instead of the conventional gas turbine cycles. While this cycle dictates additional costs for the air separation unit (ASU), it has higher thermal efficiencies than the gas turbine and combined cycles. Furthermore, it is capable to capture the excess CO_2 resulting from the combustion process and export it at a suitable pressure for commercial applications. Moreover, the DOC sCO_2 power cycle significantly reduces the amount of oxides of nitrogen (NO_x) since the combustion process is performed with pure oxygen. The NOx production rate during oxy-firing is about one-third of that during air-firing [24]. In this context, Schluckner et al. [25] developed fast and accurate CFD model for prediction of NO_x formation during the combustion of natural gas with oxygen at temperature range of 1320 °C to 1450 °C. They concluded that the partially-premixed steady flamelet model offers accurate flame shape and NO_x predictions in combination with a low computational expense. The next subsection introduces a literature review on the DOC cycles and their potential to be used in the flare gas recovery.

1.3. Potential of utilizing flare gas in DOC sCO_2 power cycles

The oxy-combustion process is one of the most promising technologies tackling CO_2 emissions from power plants powered by fossil fuels [26–28]. It was first proposed by Abraham et al. [29] in 1982 to increase oil recovery. In this process, the fuel is combusted with relatively pure oxygen provided by ASU, and most of the combustion products are recirculated into the combustor to control the combustion temperature [30]. Over the past few decades, several oxy-combustion power cycles have been proposed such as MATIANT cycle [31,32], Graze cycle [33], semi-closed oxy-combustion combined cycle (SCOC-CC) [34], and NET power cycle (Allam cycle) [35]. Currently, Allam cycle is one of the most promising DOC power cycles [36], which can capture 98.9% of the combustion products with net energy efficiency of 51.44% for gasified coal and 58.9% for NG [37,38].

Several studies in open literature have been conducted on Allam cycle to evaluate its technical, environmental, and economical characteristics and to optimize the operating conditions of its components [39–44]. These studies have been completely reviewed by the authors of the present work in their previous publications as in [45,46]. Although Allam cycle is efficient and very promising technology, its very high pressure (300 bar) and temperature (1150 °C) make the design of its components quite challenging and costly [42]. In particular, the regenerator has to handle five cold and hot streams including the turbine exhaust flow, the recycled sCO_2 flow, the oxidant, the turbine coolant flow, and the flow that transfers heat from the ASU to the regenerator to correct the thermodynamic imbalance that occurs in the regenerator. This dictates extremely large heat transfer area and robust structure to withstand the pressure differences (200–300 bar) and high temperatures (700–750 °C) [47]. Therefore, in 0this study, the outlet temperature of the combustion products was maintained at intermediated level

(550–750 °C) to simplify the design of the turbine, HTR, and LTR. Within this range, there is no need for coolant flow to cool the turbine and no need for additional heat from the ASU.

Exergoeconomic and levelized cost of electricity (LCOE) analyses, at the level of system components, thermodynamic evaluations based on energy and exergy analyses with economic principles [48–51] are necessary to obtain useful information for the design and operation of a cost-effective system. Furthermore, exergoeconomic analysis is fundamental step to compare various options of innovative cycles based on combined energetic, exergetic, and economic evaluations with advantageous ability to determine the real potential for improvement of each significant component and to consider the interactions among components [52,53]. Other researchers also evaluated the thermodynamic and exergoeconomic behavior of typical sCO₂ cycles integrated with other systems such as multi-effect desalination [54], power/cooling/heating [55,56], fuel cell [57], ORC [51,58], and geothermal [59]. Therefore, in this study, comprehensive energetic, exergetic, and economic models were developed for the proposed configurations and thorough systematic analysis is performed.

1.4. Contributions and manuscript organization

In this study, the flare gases are proposed to be used as fuel for an intercooled DOC sCO₂ power cycle. The intercooled configuration is selected for its high energy efficiency compared to other proposed configurations in literature [37,60], which can potentially achieve our very ambitious target "no flaring-no emissions". Consequently, the main objectives and contributions of the present study are:

- Proposing a new approach for the flare gas recovery by using it as a fuel for direct oxy-combustion sCO₂ power cycle to achieve "no flaring, no emissions" target.
- Proposing two novel sCO₂ power cycle configurations that utilize the flare gases as a fuel for the main heating process or for the reheating process as explained in detail in section 2.
- Conducting thorough energetic, exergetic, economic, and multi-objective optimization analyses for the proposed configurations.
- Comparing the performance of the proposed configurations for six different flare gas samples.
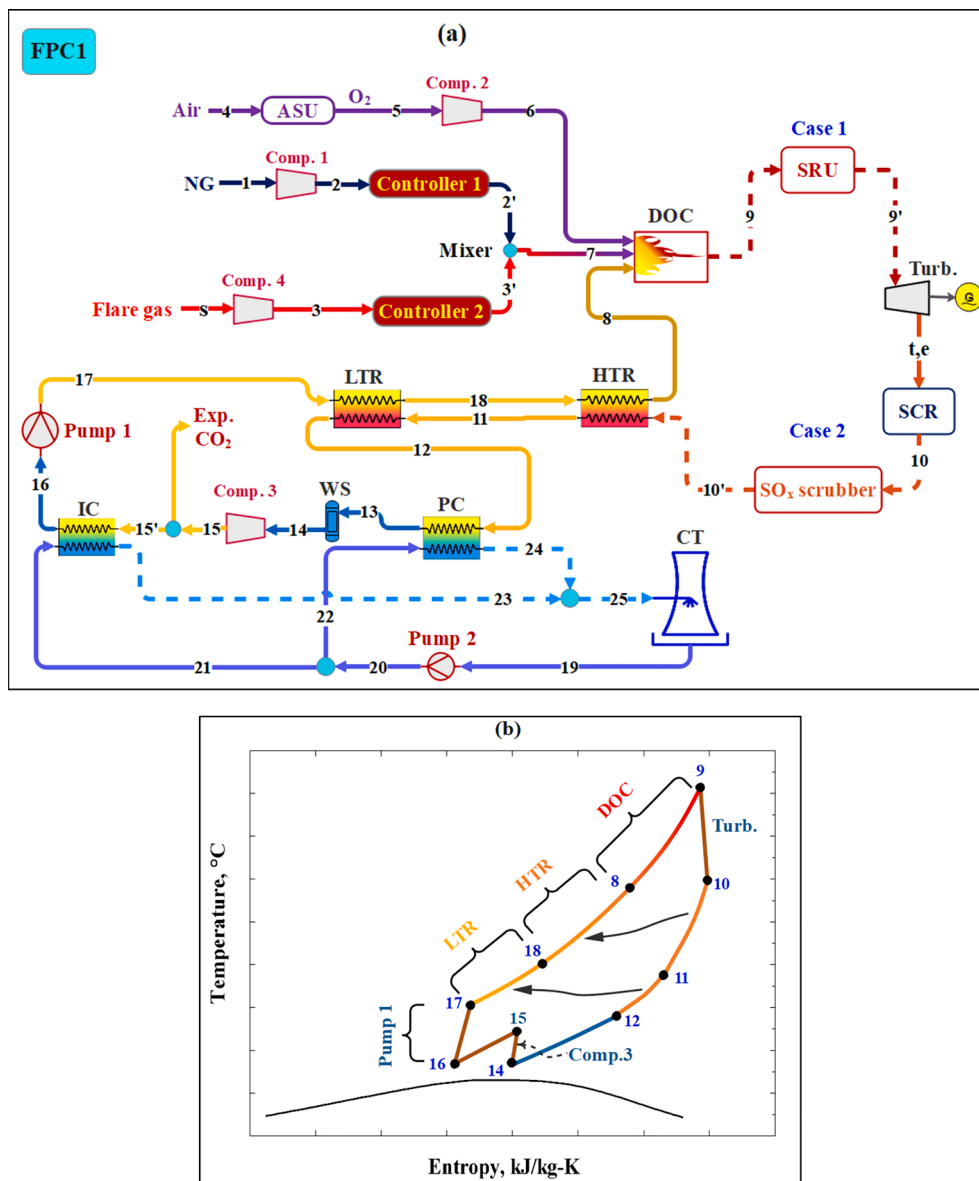

Fig. 2. (a) Schematic diagram of the flare power cycle (FPC1) in which the flare gas is mixed and combusted with the natural gas in the DOC (b) T-S diagram of FPC1.

The rest of the manuscript is organized into four more sections. Section 2 describes the proposed configurations detailing their technical characteristics and advantages. Section 3 presents the developed energetic, exergetic, and economic models and the validation results. In section 4, parametric studies are carried out for the major operating conditions including effects of maximum and minimum cycle pressures and temperatures, flare composition, and flow rates. Results of the single- and multi-objective optimization analysis are presented and discussed in subsection 4.2. The main findings and conclusions are summarized in section 5.

2. Description of the integrated flare gas sCO₂ power cycle configurations

Fig. 2 (a) and (b) depict the configuration and the T-S diagram of the first flare power cycle (FPC1) in which the flare gas is received from the flare gas recovery system (FGRS) at given pressure and temperature with variable flow rate (state "s") to be mixed with the NG. For efficient mixing of NG and flare gas, the temperature and pressure of these fuels should be the same as much as possible. Therefore, the NG is compressed by compressor 1 (1–2) and the flare gas is compressed by compressor 3 (s-3) to the operating pressure of the direct oxy-combustor (DOC). To maintain stable operation for the combustor, the FPC1 system operates in a way that the fuel flow rate at the inlet of the DOC is maintained constant by both controller 1 and controller 2. At a high flare flow rate, only flare gas is used and controlled via controller 2 while the NG flow is paused by controller 1. When the flare flow rate becomes lower, an appropriate amount of the NG is mixed to compensate for it. The required amount of oxygen needed for the oxy-combustion process is provided by the ASU (4–5) and compressed to the combustor pressure in compressor 2 (5–6). To control the temperature of the combustion products, part of the supercritical CO₂ is recycled to the DOC (state 8). At state 9, the combustion products (CO₂, H₂O, SOₓ, NOx, and N₂) leave the combustor at an intermediate temperature (550 °C to 750 °C) and high pressure (200 bar to 300 bar) to expand in the turbine (9′-10′). As most of the flare gases contain significant amount of H₂S, a removal process of H₂S is necessary. This can be achieved using one of two different methods: Case 1: H₂S is removed via a Sulfur recovery unit (SRU) installed before the turbine (9–9′); and Case 2: H₂S is removed via a SOₓ scrubber unit installed at the exit of the turbine (10–10′). Case 1 has considerable capital and operating costs while Case 2 imposes that the sour gas enters the turbine, which has corrosive effect on the turbine blades. Therefore, a material factor should be considered in the evaluation of the turbine costs, which is contemplated in the thermoeconomic model in section 3.3.

Due to the presence of nitrogen (N₂) in the flare gases, nitrogen oxides (NOx) will be formed and existed within the flow at the outlet of the combustor. However, since the combustor works at moderate temperatures, the formation of NOₓ is much smaller than those formed in conventional combustors. But, the high pressure of the combustor boosts the formation of acid gases such as NO₂ and SO₂ [61]. Therefore, the selective catalytic reduction (SCR) process is considered to remove NOₓ [62,63] at the exit of the turbine (process t,e – 10). Even with those emission treatments, a small percentage of N₂ (less than 0.61%vol. as average value for all studied samples in this work) still existed in the inlet of the HTR. This percentage is acceptable in the exported CO₂ according to the CO₂ quality specifications reported by many CO₂ transportation projects such as Canyon Reef project [64,65]. For oxy-fuel combustion technologies, N₂ impurities is acceptable up to 4%vol. as recommended by Dynamis project [66]. Thus, the target of this work "no flaring-no emissions" seems to be achievable as all the harmful emissions (SOₓ and NOₓ) being removed and extra CO₂ is exported in acceptable quality for commercial applications or sequestrated in an appropriate location. After eliminating SOₓ and NOₓ from the combustion products (before or after the turbine), the remaining flow is composed only from sCO₂ and water vapor and negligible percent of N₂.

The turbine exhaust flow enters the HTR (10″–11) and LTR (11–12) to preheat the recycled sCO₂. Then, the hot stream flows through the precooler PC (12–13) and water separator WS (13–14). The precooler works on wet cooling conditions using cooling towers to realize the dense phase of the sCO₂ at the inlet of the compressor. However, water evaporation losses in cooling towers account for a considerable amount of freshwater consumption [67]. Therefore, the dry cooling method can be used with the penalty of more compression power consumption by the cycle compressors [45,46]. At state 14, the sCO₂ fluid is compressed by compressor 3 (14–15) to an intermediate pressure. At the exit of Comp. 3, the excess sCO₂ produced in the combustion process is exported and the remaining part is cooled again by the intercooler IC (15–16) to state 16 (which is near the critical state of the carbon dioxide 30.9 °C and 73.9 bar). At state 16, the sCO₂ exists in a dense phase and could be pumped by pump 1 (16–17) to the desired pressure. Using the pump instead of the gas compressor significantly reduces the compression power. Then, the high pressurized CO₂ flow is recycled to the DOC after being preheated by the LTR (17–18) and the HTR (18–8) to repeat the cycle as presented in the T-S diagram of FPC1 (Fig. 2 (b)).

Another way to use the flare gas is illustrated in the configuration of the second flare power cycle (FPC2) as shown in Fig. 3 (a). In FPC2, the flared gas is used to perform reheating process in the reheater (10–9′) for the exhaust flow turbine 1 to generate additional power by turbine 2 (9′–10′). Similar to FPC1, the SOₓ are removed either by the SRU (Case 1) or by SOx scrubber (Case 2) and the NOₓ are removed by SRC. Since the flow rate of the flare is variable with respect to time, controller 3 is connected with the NG line (which is controlled by controller 1) to compensate for any reduction in the required amount of fuel for the reheater (at state rh,i). After eliminating SOₓ and NOₓ from the combustion products, the exhaust flow of turbine 2 enters the HTR at state 10″ to repeat the same processes as in FPC1.

3. Thermodynamic, exergoeconomic, and thermoeconomic modeling

This section describes the energetic, exergetic, and economic models that were developed for the analysis of the proposed flared sCO₂ power cycles. Throughout the analysis, steady state operation is assumed and the variations of the kinetic and potential energies are neglected.
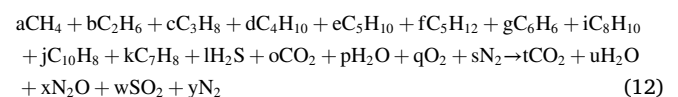
3.1. Thermodynamic models

3.1.1. Energy model

The energy models of the proposed flare GTP sCO₂ cycle configurations were developed by applying the mass and energy conservation principles on the control volume of each component such that [46,58]:

$$\sum \dot{m}_i = \sum \dot{m}_o \qquad (10)$$

$$\sum \dot{Q} + \sum \dot{m}_i h_i = \sum \dot{W} + \sum \dot{m}_o h_o \qquad (11)$$

The details of the mass and energy balance equations of each component of the cycle configurations are provided in the supplementary material (Table SM.1). The mass flow rate of the oxygen required for the oxy-combustion process and the mass flow rate of the CO₂ at the exit of the combustor were calculated based on the real combustion reaction as follows [22]:

$$aCH_4 + bC_2H_6 + cC_3H_8 + dC_4H_{10} + eC_5H_{10} + fC_5H_{12} + gC_6H_6 + iC_8H_{10}$$
$$+ jC_{10}H_8 + kC_7H_8 + lH_2S + oCO_2 + pH_2O + qO_2 + sN_2 \rightarrow tCO_2 + uH_2O$$
$$+ xN_2O + wSO_2 + yN_2 \qquad (12)$$

The heat exchangers (LTR, HTR, IC, and PC) were modeled based on the effectiveness method using Eq. (13) [46,68] where variable specific heat of the CO₂ as a function of temperature is taken into consideration as detailed in Sleiti and Al-Ammari [46].
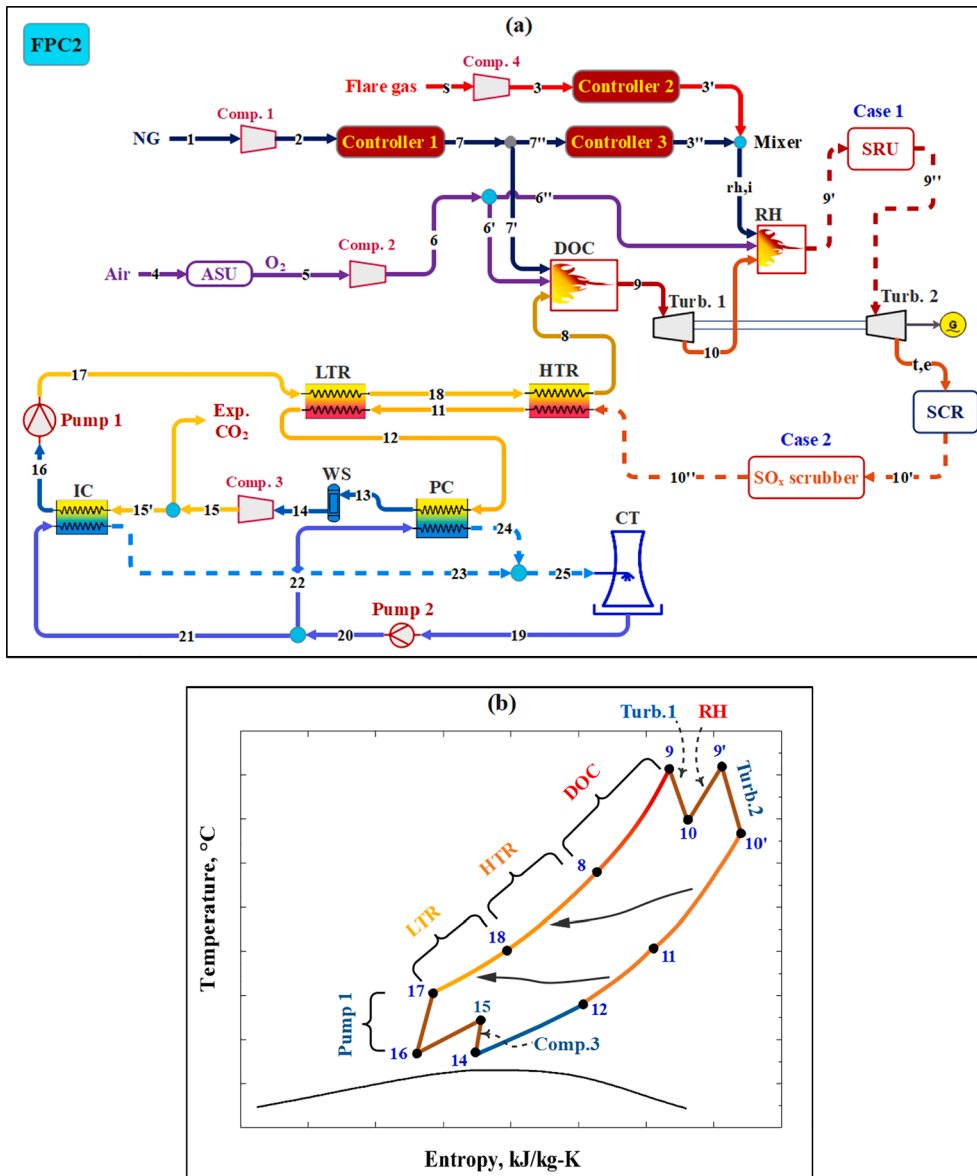
Fig. 3. (a) Schematic diagram of the flare power cycle in which the flare gas burned separately in a reheater (FPC2) (b) T-S diagram of FPC2.

$$\in = \frac{\dot{Q}}{\dot{Q}_{max}} \quad (13)$$

The thermal efficiency of each configuration is expressed in terms of the net output power ($\dot{W}_{net}$) and the total input power ($\dot{Q}_{in}$):

$$\eta_{th} = \frac{\dot{W}_{net}}{\dot{Q}_{in}} \quad (14)$$

where the equations of $\dot{W}_{net}$, and $\dot{Q}_{in}$ are given in Table SM.1

3.1.2. Exergy model

The exergy model of the proposed configurations was developed by applying the second law of thermodynamics on the control volume of each component such that:

$$\dot{E}_Q + \sum \dot{E}_i = \dot{E}_W + \sum \dot{E}_o + \dot{E}_D \quad (15)$$

Neglecting the changes of the kinetic and potential exergies, the exergy of each stream is calculated as the sum of the physical ($\dot{E}_{ph}$) and chemical ($\dot{E}_{ch}$) exergies:

$$\dot{E} = \dot{E}_{ph} + \dot{E}_{ch} \quad (16)$$

The physical and chemical exergies are given as [46,69]:

$$\dot{E}_{ph} = \dot{m}((h - h_o) - T_o(s - s_o)) \quad (17)$$

$$\dot{E}_{ch} = \dot{n}[\sum_{j=1}^{n} x_j e_j^o + RT_o \sum_{j=1}^{n} x_j \ln(x_j)] \quad (18)$$

where $\dot{n}$ is the molar flow rate, x_j is the molar fraction of jth component in a mixture, and e_j^o is the standard chemical exergy of jth component at T_o and P_o conditions. In this study, the fuel-product-loss method is used to evaluate the exergy efficiency of each layout component and the overall exergy efficiency of each configuration. For kth component, the balanced equation of fuel-product-loss exergies and its exergy efficiency are given in Eq. (19) and Eq. (20), respectively [52,70]. The definitions of the fuel and product exergies for each component of the proposed cycles are presented in the supplementary material (Table SM.2) [30].

$$\dot{E}_{D,k} = \dot{E}_{F,k} - \dot{E}_{P,k} - \dot{E}_{L,k} \quad (19)$$

$$\varepsilon_k = \frac{\dot{E}_{P,k}}{\dot{E}_{F,k}} \tag{20}$$

The overall exergy efficiency of each system is:

$$\varepsilon_{overall} = \frac{\sum \dot{E}_{P,k}}{\sum \dot{E}_{F,k}} \tag{21}$$

3.2. Exergoeconomic model

The exergoeconomic analysis combines exergy and economic analyses at the level of the system components [54]. In this study, the exergoeconomic model is built to obtain product cost per unit exergy. The general cost balance equation is applied to each component to obtain the cost rate of each stream, which is given as:

$$\sum \dot{C}_{out,k} + \dot{C}_{po,k} = \sum \dot{C}_{in,k} + \dot{C}_{q,k} + \dot{Z}_k \tag{22}$$

where $\dot{C}_{in,k}$, and $\dot{C}_{out,k}$ are the cost rates of inlet and outlet streams of the component. $\dot{C}_{q,k}$, and $\dot{C}_{po,k}$ are the cost rates related to the thermal energy input and power output of the component (if existed). $\dot{Z}_k$ is the sum of capital investment, maintenance, and operating costs, which is expressed as in Eq. (23) [55].

$$\dot{Z}_k = \left(\frac{CRF}{\tau}\right) Z_k + \gamma_k Z_k / \tau \tag{23}$$

where Z_k is the capital cost of each component which is presented in the supplementary material (Table SM.3). γ_k is the weighting coefficient (fixed at 0.06) and τ is the plant operation time per year (7446 hrs). The CRF is the capital recovery factor which is related to the interest rate ($\omega = 12\%$) and the lifetime of the plant ($n = 20 years$):

$$CRF = \frac{\omega \bullet (1 + \omega)^n}{(1 + \omega)^n - 1} \tag{24}$$

The total product unit cost ($c_{P,total}$) is calculated as:

$$c_{P,total} = \frac{\sum_{i=1}^{n_k} \dot{Z}_k + \sum_{i=1}^{n_f} c_f \dot{E}_F}{\sum_{i=1}^{n_p} \dot{E}_P} \tag{25}$$

The cost balance equation for each component of the proposed configurations are presented in the supplementary material (Table SM.4).

3.3. Thermoeconomic model

The economic evaluation of the proposed configurations is performed in terms of the LCOE, which is calculated according to Eq. (26) [71].

$$LCOE = \frac{PC - PV_{DTS} + PV_{LOC} - PV_{SC}}{LEP} \tag{26}$$

where PC is the project cost which is the sum of the components and installation costs (given in Eq. (27)), PV_{DTS} is the present value of the depreciation tax shield (given in Eq. (28)), PV_{LOC} is the present value of lifetime operating costs (given in Eq. (29)), PV_{SC} is the present value of salvage costs (assumed $0.00), and LEP is the lifetime electrical production (given in Eq. (30)).

$$PC = \sum \left(Component cost + Installation cost\right)_k \tag{27}$$

$$PV_{DTS} = TR \times PC / (1 + DR)^{DP} \tag{28}$$

$$PV_{LOC} = n^*(OMC + Cost of the fuel) / (1 + DR)^n \tag{29}$$

$$LEP = PUF \times n \times \dot{W}_{net} \times 8760 \tag{30}$$

where TR is the tax rate (35%), DR is the discount rate (2%), DP is the depreciation period (10 years), n is the lifetime of the plant (20 years), and PUF is the plant utilization factor (85%). Table SM.3 presents the capital cost functions of each component while the installation and direct labor costs were taken as 12% of the capital component cost [72].

3.4. Solution procedures

Table 2 shows the input parameters for the analysis of the proposed configurations including sCO$_2$ cycle parameters, pressure drops through components, and the parameters of the economic evaluation. The energy, exergy, exergoeconomic, and thermoeconomic models for each configuration are coded and solved in the Engineering Equation Solver (EES) software (based on the procedures shown in Fig. 4) and the thermodynamic properties were obtained from its library. Then, single- and multi-objective optimization are performed using genetic algorithm (GA). GA method was chosen among several other optimization methods because of its robustness and is not affected by the guessed initial values like the other methods [54,73,74].

To evaluate the potential of the flare gases for power generation in direct oxy-combustion cycles, a careful examination must be conducted for the available different flare gas samples from different sources to determine the most appropriate option from energetic, exergetic, and economic point of views. Therefore, six flare gas samples from different sources with various specifications and compositions, [23], were investigated in this study. Table 3 shows the conditions and the compositions of the flare samples, which include four upstream (associated gas) samples and two downstream (from gas refineries) samples. It is worth mentioning that the composition of downstream flare gases from oil refineries has high hydrogen content (35% to 70%), which significantly reduces their heating values and increases the formation of SOx; thus, yields higher capital and operational costs [23]. Therefore, the flare gases from oil refineries that have high hydrogen content are not investigated in this study.

As shown in Table 3, Sample 4 has the highest flow rate among the other samples, which makes it appropriate source for the generation of the designed capacity (50 MW) without using additional NG as will be

Table 2
Design point parameters.

|	Parameter	Range/Design value
sCO$_2$ power cycle parameters	Net output power, $\dot{W}_{net}$ (MW)	50
	Maximum cycle pressure, P_{max} (bar)	200–300/250
	Minimum cycle pressure, P_{min} (bar)	33–40/33
	Minimum cycle temperature, T_{min} (°C)	32–50/32
	Turbine isentropic efficiencies, (%) [52]	93
	Compressor isentropic efficiencies, (%) [75]	85
	Lower heating value of natural gas, LHV_{NG}(kJ/kg) [76]	50,500
	Pressure drops across the DOC, (%) [77]	3
	Pressure drops across the HTR and LTR (hot side), (%) [77]	3
	Pressure drops across the HTR and LTR (cold side), (%) [42]	1
	Pressure drops across the PC and IC, (%) [42]	2
	Specific power consumption of the ASU, SPC_{ASU}, (kWh/kg$_{O2}$) [78]	250
Economic parameters	Plant lifetime, n (years)	20
	Depreciation period, DP (years)	10
	Tax rate, TR (%)	35
	Plant utilization factor, PUF (%)	85
	Cost of the fuel, ($/kWh$_e$)	0.086
	Operation and maintenance cost, ($/kWh$_e$)	0.008
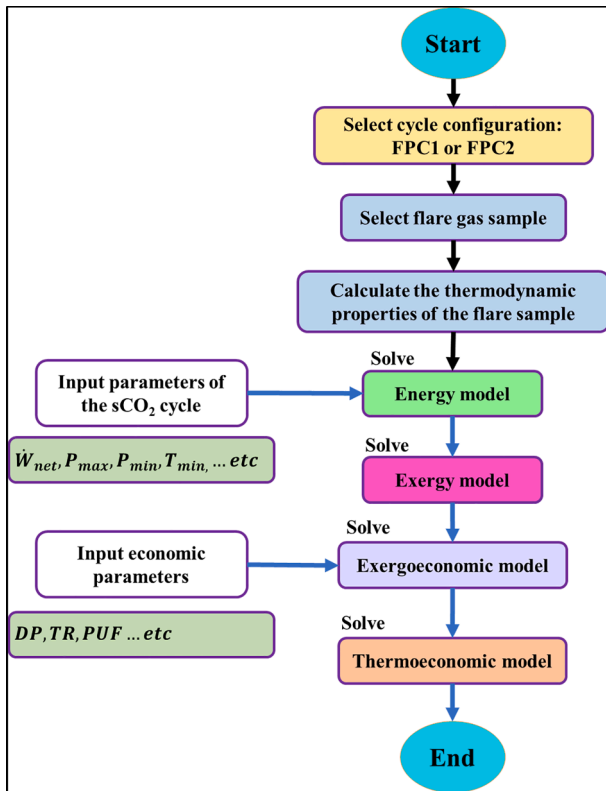
Fig. 4. Flow chart of the solution procedures.

shown in the results section. In contrast, the flow rate of the other samples is much lower than the demand for a net output power of 50 MW, which necessitates mixing the flare gas with NG to provide the required amount of fuel. Since the heating value of the NG is higher than that of the flared gas, it is expected that the samples with a lower flow of the flare will gain higher thermal efficiencies (at fixed output power). The high heating value of the NG makes it possible to reach the design turbine inlet temperature with a lower fuel flow rate and lower recycled sCO_2, which accordingly reduces the consumed power by the compressors and ASU and improves their thermal efficiencies (This will be discussed in detail in section 4). Moreover, the temperatures and pressures of the investigated samples impose different power consumption to compress them to the desired operating pressure of the combustor. Furthermore, samples 1 and 5 are sweet and did not need SOx removal units, which increases their potential from an economic point of view. Due to the dramatic changes between the specifications of these samples, comprehensive and systematic simulations were performed for

each of them in both proposed cycle configurations (FPC1 and FPC2).

3.5. Verification and validation of the model

To verify and validate the developed models for the direct oxy-combustion cycles and to verify the accuracy of the thermodynamic properties obtained from EES library, verification and validation processes are performed as follows:

The accuracy of the thermodynamic properties and solution results of the developed codes were verified by writing special codes for the simple and recompression sCO_2 power cycles that were investigated by Dyreby et al. [79]. Then, these codes were run under the same operating conditions to estimate the required mass flow rate and the thermal efficiency of each cycle. The input parameters and the results are presented in Table 4. It can be noted that the error between the simulated results in this study and those reported by [79] does not exceed 0.8%. However, this error may be attributed to the analysis method of the recuperators. In this study, we have performed discretized analysis for the calculations of the recuperators as detailed in Sleiti et al. [46]. The discretized analysis of the recuperators is more accurate and results in lower recovered heat by the recuperators than the obtained by the average-based calculations and hence, the required heat in the primary heater is increased. This explains why the obtained thermal efficiencies in the present study (Table 4) are slightly lower than reported in [79].

The above verification process was conducted for closed sCO_2 power cycles (which use pure CO_2 as a working fluid), however, the working fluid of the DOC cycles considered in the present study is a mixture of CO_2, H_2O, SO_x, and NO_x. So, it is necessary to perform additional validation of the developed models in this study for the DOC sCO_2 power cycles. However, there is no available data in the open literature for the DOC sCO_2 power cycles that are powered by flare gases or a mixture of flare gases and NG. Therefore, the additional validation of the present study is performed by comparing the results obtained by our DOC sCO_2 cycles (with NG only) with data for the Allam cycle (which is a DOC sCO_2 power cycle) reported by Scaccabarozzi et al. [42]. The model of FPC1 is slightly modified to fit the configuration of the Allam cycle and the operating conditions (inputs) were adjusted to be the same as in [42]. Table 5 shows the results obtained by our model compared to [42]. It can be noted that the maximum residual error is −3.85% associated with the turbine outlet temperature. The main reason for this difference is attributed to the slight difference in the composition of the exhaust flow from the combustor between the present study and Scaccabarozzi et al. [42]. However, the error of the net electric efficiency does not exceed 1%, which is considered sufficient for the validation of the proposed model.

Table 3
Specifications and composition of the investigated flare samples. Adapted from [23].

Conditions	Upstream (associated gas)				Downstream (gas refineries)	
	Sample 1	Sample 2	Sample 3	Sample 4	Sample 5	Sample 6
Temperature, (°C)	37.00	45.00	68.00	41.35	30.27	19.00
Pressure (bar)	1.08	5.00	5.00	1.20	8.00	1.00
Flow rate, (kg/s)	0.18	1.09	2.95	4.50	0.19	0.62
Heating Value, (kJ/kg)	25,452	37,726	29,808	29,342	21,890	14,205
Compositions, (molar %)						
Methane, (CH_4)	85.47	66.74	66.26	64.24	91.00	62.53
Ethane, (C_2H_6)	9.16	13.11	13.02	15.82	3.46	0.36
Propane, (C_3H_8)	3.48	6.31	6.26	8.81	0.95	0.06
Higher Hydrocarbons, (C_{4+})	1.89	13.84	13.75	11.13	0.89	0.15
Water, (H_2O)	0.00	0.00	0.00	0.94	0.06	0.00
Hydrogen Sulfide, (H_2S)	0.00	0.71	0.70	1.27	0.00	5.38
Carbon Dioxide, (CO_2)	0.33	0.00	0.00	2.05	0.44	29.54
Nitrogen, (N_2)	0.07	0.02	0.02	0.64	3.10	1.80

Table 4
Verification of codes and calculations compared to the result reported by Dyreby et al. [79] for simple and recompression sCO$_2$ power cycles.

Items	Simple sCO$_2$ power cycle			Recompression sCO$_2$ power cycle		
	Ref. [79]	Present study	Error (%)*	Ref. [79]	Present study	Error (%)*
$\dot{W}_{net}$, (MW)	10	10	N.A-Input	10	10	N.A-Input
UA_{LTR}, (kW/°C)	1500	1500	N.A-Input	677	677	N.A-Input
UA_{HTR}, (kW/°C)	N.A**	N.A**	N.A**	823	823	N.A-Input
P_{min}, (MPa)	8.14	8.14	N.A-Input	9.17	9.17	N.A-Input
P_{max}, (MPa)	25	25	N.A-Input	25	25	N.A-Input
T_{min}, (°C)	45	45	N.A-Input	45	45	N.A-Input
T_{max}, (°C)	700	700	N.A-Input	700	700	N.A-Input
$\dot{m}_{CO_2}$, (kg/s)	77.40	77.40	0.00	85.80	85.99	−0.22
η_{th}, (%)	47.6	47.26	0.71	49.40	49.17	0.47

* Error (%) = 100*(Ref. [79] value – Present study value)/ Ref. [79] value;
** N.A = Not applicable for the simple sCO2 power cycle.

Table 5
Validation results of the proposed model compared to results published by Scaccabarozzi et al. [42].*

Items	Ref. [42]	Present work	Error (%)*
Net electrical power output (MW$_e$)	419.31	419.31	N.A-Input
Thermal energy of the fuel (LHV) (MW$_{th}$)	768.31	775.20	−0.89
Turbine power output (MW)	622.42	637.20	−2.37
Recycle flow compression (MW)	111.15	112.86	−1.54
NG compressor consumption (MW)	4.18	4.32	−3.35
ASU penalty (MW)	85.54	83.86	1.90
Turbine outlet temperature (°C)	741.2	769.6	−3.83
Recycle flow final temperature (°C)	721.2	734.8	−1.89
Turbine inlet flow rate	1271	1268	0.24
Total recycle flow rate (with O$_2$) (kg/s)	1353.9	1353.5	0.03
Net electrical efficiency (%)	54.58	54.09	0.90

At T_1 = 1150 °C, T_6 = 26 °C, P_1 =,300 bar and P_6 = 32.2 bar.
* Error (%) = 100*(Ref. [42] value – Present study value)/ Ref. [42] value;

4. Results and discussion

4.1. Sensitivity analysis

The sensitivity analysis is performed by investigating variations of the energetic, exergetic, and economic (EEE) performance indicators (which are the thermal efficiency, exergy efficiency, total product unit cost, and the LCOE of each configuration) with the variation of the major operating conditions including the maximum cycle pressure (section 4.1.1), minimum cycle pressure (section 4.1.2), maximum and minimum cycle temperatures (sections 4.1.3 and 4.1.4), and the flare composition and specifications (section 4.1.5).

4.1.1. Effect of the maximum cycle pressure

Fig. 5 shows how the EEE performance indicators of cycle configuration FPC1 change with the increase of the maximum cycle pressure (P_{max}) including the thermal efficiency Fig. 5(a), overall exergy efficiency Fig. 5(b), total product unit cost Fig. 5(c), and LCOE Fig. 5(d). The thermal efficiency of FPC1, Fig. 5(a), decreases with the increase of P_{max} for all flare gas samples except sample 4, which maintains constant efficiency over the investigated range of P_{max} (200 to 300 bar). At fixed T_{max} of 750 °C and exit turbine pressure of 34.24 bar, the increase of P_{max} yields lower temperature at the turbine exit, which minimizes the

recuperated heat by the HTR and LTR. Therefore, a lower temperature is obtained at the inlet of the DOC, which requires more NG to reach the desired T_{max} and reduces the thermal efficiency of FPC1 (by 7.53% over the range of P_{max}). However, due to the large flow rate of sample 4 (4.5 kg/s), it does not consume any NG for the 50 MW FPC1 capacity. Therefore, over the investigated range of P_{max}, the available amount of flare flow of sample 4 is enough to be combusted (fixed input thermal energy) to provide the desired net output power of 50 MW, which yields constant efficiency. When the capacity increases to 100 MW, however, the behavior of sample 4 becomes the same as the other samples as it requires additional NG to compensate for the needed input thermal energy of the combustor to achieve that capacity of 100 MW. Furthermore, it is noticed that the flare samples with a lower flow rates (Samples 1, 2, 5 and 6) provide higher thermal efficiencies as shown in Fig. 5 (a). Although the lower flare flow rate means more NG is needed, the higher heating value of NG makes it possible to reach the desired T_{max} with lower recycled sCO$_2$ which significantly reduces the consumed power by Pump 1 and improves the thermal efficiency of these samples. In contrast, samples 3 and 4 require higher flow of the recycled sCO$_2$ (due to the larger heat input associated with the larger flare flow rate) to moderate the temperature at the turbine inlet. Therefore, compared to the other samples, the compression power of Pump 1 associated with samples 3 and 4 is increased by 10.9% and 19.3%, respectively. Consequently, the thermal efficiencies of samples 3 and 4 are lower than of the other samples by 2.1% and 17.4%, respectively.

Fig. 5(b) shows the variation of the overall exergy efficiency ($\varepsilon_{overall}$) of FPC1 with the increase of P_{max}. The increase of P_{max} increases the temperature at the outlet of pump 1 and the inlet of the precooler (PC) and reduces the temperature at the inlet of the DOC. This in turn elevates the exergy destruction of these components and reduces the $\varepsilon_{overall}$ (by 2.36% over the range of P_{max}). In contrast to the thermal efficiency, samples with higher flare flow rates have higher $\varepsilon_{overall}$. This is explained by that the exergy efficiency of the DOC is improved at a higher flare flow rate as the fuel exergy of the DOC at higher flare flow is lower than at lower flare flow. However, the deviation between the $\varepsilon_{overall}$ of the flare samples is much smaller than the deviation between their thermal efficiencies. This means that the exergy destruction rate depends on the components' design rather than the flare composition. Thus, improving the performance of the components is essential to enhance the exergetic performance of the cycle. Fig. 5(c) shows the total product unit cost ($c_{p,total}$) of the investigated samples is almost constant with the increase of P_{max}. This interpreted by that $c_{p,total}$ depends on both energetic and exergetic performances of the cycle. As those performances have opposite behavior with the increase of P_{max}, the sensitivity of $c_{p,total}$ for P_{max} is minimized. However, it shows that the sample with higher $\varepsilon_{overall}$ has lower $c_{p,total}$. Over the design range of P_{max}, Fig. 5(d) illustrates that the LCOE of FPC1 decreases as P_{max} increases (by 16.2% over the range of P_{max}). This is attributed to the decrease of the thermal loads of the HTR, LTR, PC, and IC, which minimizes their capital and operational costs. Obviously, samples that have higher thermal efficiency yield lower LCOE due to the reduction of the total compression power, which forms more than 50% of the gross turbine power.

Fig. 6 shows the effect of P_{max} on the thermal efficiency Fig. 6(a)), overall exergy efficiency (Fig. 6(b)), total product unit cost (Fig. 6(c)), and LCOE (Fig. 6(d)) for FPC2. In contrast to FPC1, the thermal efficiency of FPC2 increases with the increase of P_{max} (by 9.6% for samples 1,5 and 6 and by 1.9% for samples 2,3, and 4). This is explained by that the temperature at the exit of Turbine 2 does not decrease with the increase of P_{max} (at fixed intermediate and low pressures). Therefore, the recuperated heat increases and improves the thermal efficiency with the increase of P_{max}. However, the total input power for both DOC and RH is higher than in FPC1, which makes the thermal efficiencies of the flare gas samples in FPC2 lower than in FPC1. Also, this makes the LCOE of FPC2 higher than that of FPC1 (Fig. 6(d)). For instance, at the design point conditions, η_{th} and LCOE of sample 4 in FPC1 are 37.87% and
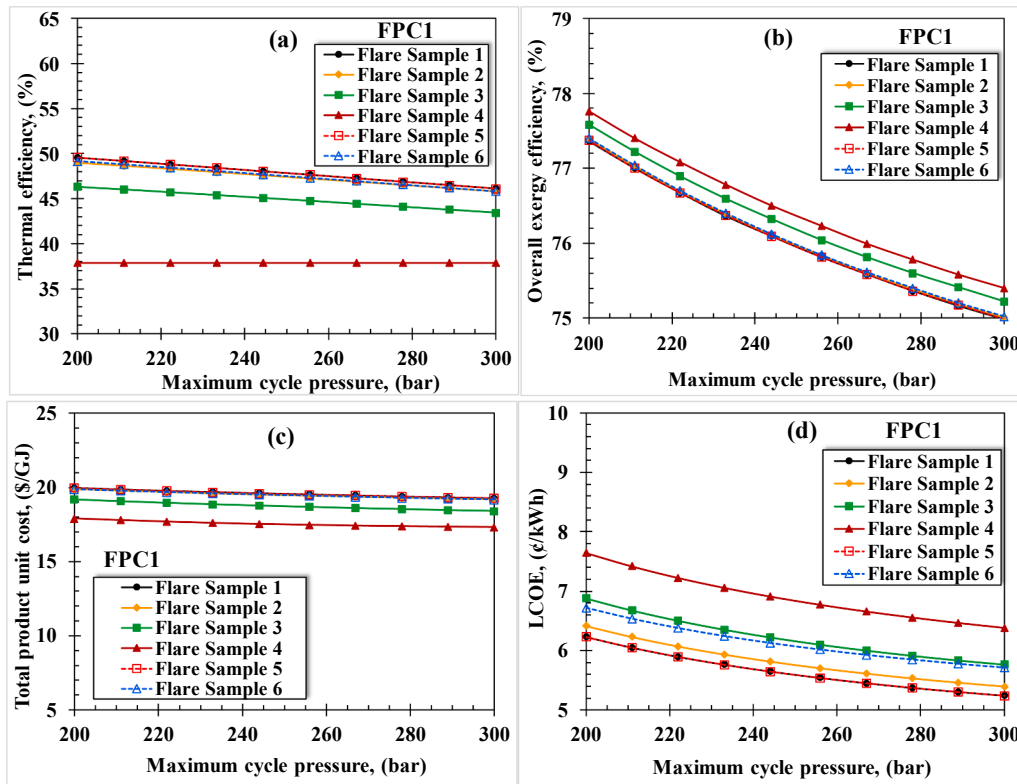
Fig. 5. Effect of the maximum cycle pressure of FPC1 on the (a) thermal efficiency, (b) exergy efficiency, (c) total product unit cost, and (d) LCOE.
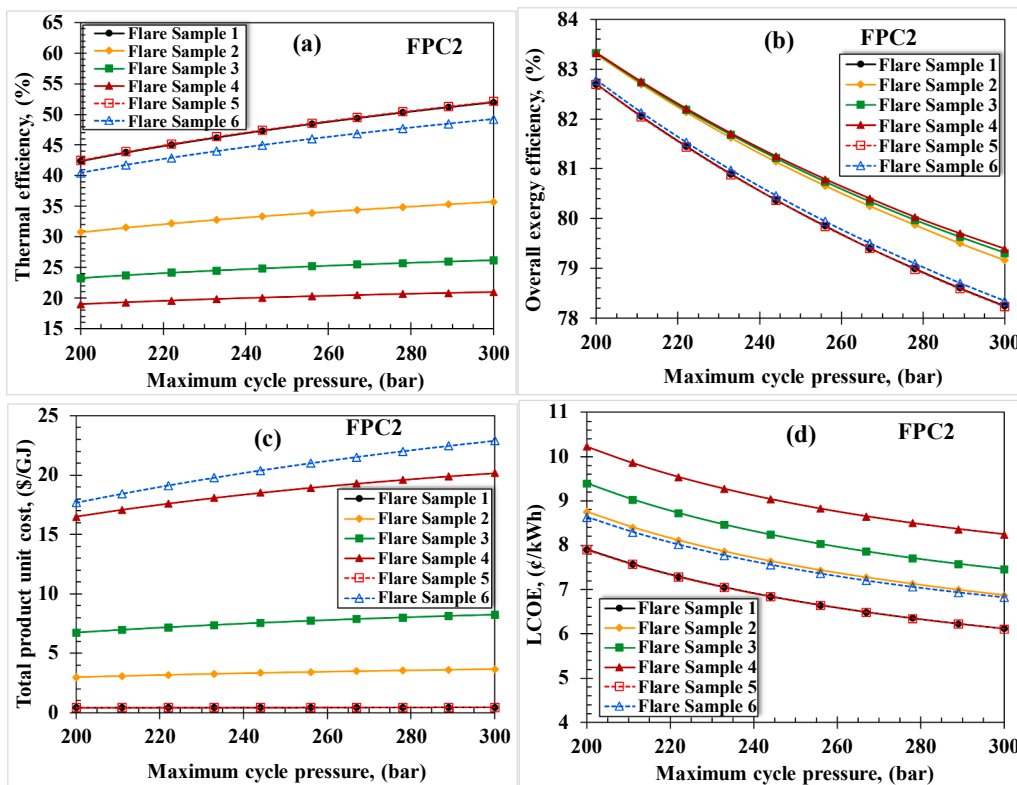

Fig. 6. Effect of the maximum cycle pressure of FPC2 on the (a) thermal efficiency, (b) exergy efficiency, (c) total product unit cost, and (d) LCOE.

6.77¢/kWh while in FPC2 they are 20.16% and 8.83¢/kWh, respectively. To improve η_{th} and minimize the LCOE of FPC2 compared to FPC1, the cycle capacity should be increased as will be discussed in

section 4.1.5. On the other hand, $\varepsilon_{overall}$ of FPC2 is higher than of FPC1 and $c_{p,total}$ of FPC2 is lower than of FPC1 for all samples as shown in Fig. 6 (b and c). This is attributed to the that the exergy destructed by the DOC

in FPC2 is much lower than in FPC1 since the DOC in FPC2 burns pure methane (natural gas), which minimizes the irreversibility associated with the chemical reactions and mixing processes. While $c_{p,total}$ decreases with the increase of P_{max} in FPC1, the opposite is true for FPC2; as the energetic performance of FPC2 is improved with the high-pressure increase.

In general, the increase of P_{max} reduces η_{th} of FPC1, improves η_{th} of FPC2, and reduces the LCOE of both FPC1 and FPC2. Further, the power plant capacity should be increased to improves η_{th} of FPC2 compared to FPC1. Moreover, flare gas samples with lower flow rates have higher η_{th} than those with higher flow rates.

4.1.2. Effect of the minimum cycle pressure

Fig. 7 describes the relationship between the minimum cycle pressure (P_{min}) and the thermal efficiency Fig. 7(a), overall exergy efficiency Fig. 7(b), total product unit cost Fig. 7(c), and LCOE Fig. 7(d) of FPC1.

As P_{min} increases, the temperature at the turbine exit also increases (for fixed $P_{max} = 250 bar$) which enhances the recuperated heat and the temperature of the recycled sCO$_2$ at the inlet of the DOC. This in turn minimizes the consumed natural gas by the combustor and reduces the cooling loads of the PC and IC. Furthermore, it reduces the compression power of Comp.3 and Pump 1 and lowers the amount of the recycled sCO$_2$. Therefore, η_{th} of FPC1 is improved (by 23%) with the increase of P_{min} (except for sample 4) as shown in Fig. 7(a). In addition, the increase of P_{min} minimizes the temperature differences between the cold and hot streams of the HTR and LTR and reduces the temperature difference across the DOC, which consequently improves the $\varepsilon_{overall}$ of FPC1 (by 2.5%) as shown by Fig. 7(b). At the same time, the increase of the recuperated heat with P_{min} imposed higher heat transfer areas and higher costs per unit exergy for the HTR and LTR. This explains why $c_{p,total}$ increases with the increase of P_{min} (see Fig. 7(c)). However, the cost reductions associated with the thermal efficiency improvement are the dominant factor which minimizes the LCOE with the increase of P_{min} as shown in Fig. 6(d). A minimum LCOE of 5.24¢/kWh for samples 1 and 5 at $P_{min} = 40$ bar and a maximum LCOE of 6.84¢/kWh for sample 4 at $P_{min} = 32$ bar were observed.

For FPC2, the effect of increasing P_{min} on the performance indicators (η_{th}, $\varepsilon_{overall}$, $c_{p,total}$, and LCOE) is noted to be similar to that of FPC1 as shown in Fig. 8. However, sample 2 achieves higher thermal efficiency at P_{min} higher than 33 bar (Fig. 8(a)). This owned to the high pressure of sample 2 at moderate flow rate which reduces the compression power of Comp. 4. The sweet samples (samples 1 and 5) have the lowest LCOE with an average of 6.71¢/kWh as shown in Fig. 8(d). This is because that the cost of SO$_x$ treatment is eliminated as these samples contains no hydrogen sulfide. Furthermore, the increase of the exergy efficiency of FPC2 with P_{min} (Fig. 8(b)) compensates for the increase of the capital and operational costs, which makes $c_{p,total}$ almost constant over the range of P_{min} (Fig. 8(c)). In this context, Sample 4 has the highest $c_{p,total}$ among the other samples which resulted by the higher concentration of H$_2$S.

4.1.3. Effect of the maximum cycle temperature, T_{max}

Fig. 9 presents the effect of T_{max} of FPC1 on the thermal efficiency (Fig. 9(a)), overall exergy efficiency (Fig. 9(b)), total product unit cost (Fig. 9(c)), and on the LCOE (Fig. 9(d)). As the design T_{max} at the inlet of the turbine increases, the amount of the recycled sCO$_2$ decreases, leading to a reduction in both the consumed fuel and the compression power and improves η_{th}. This increase in η_{th} is about 24.6% over the range of T_{max} for all six samples except 4, Fig. 9(a). However, η_{th} of sample 4 keeps increasing up to T_{max} of 694 °C then levelized due to the limitations of the available flare flow rate. Controversially, the $\varepsilon_{overall}$ decreases as T_{max} increases, Fig. 9(b), as the temperature differences across the recuperators and the coolers of the cycle are increasing too. Consequently, the $c_{p,total}$ increases up to T_{max} of 672 °C then decreases, since the decrease of the product exergies becomes less than the decrease of the fuel exergies especially for the cycle heat exchangers (HTR, LTR, PC, and IC). The LCOE decreases with the increase of T_{max} up to an optimum value of T_{max} then increases at higher temperatures. This is because the high operating temperatures increase the capital costs of
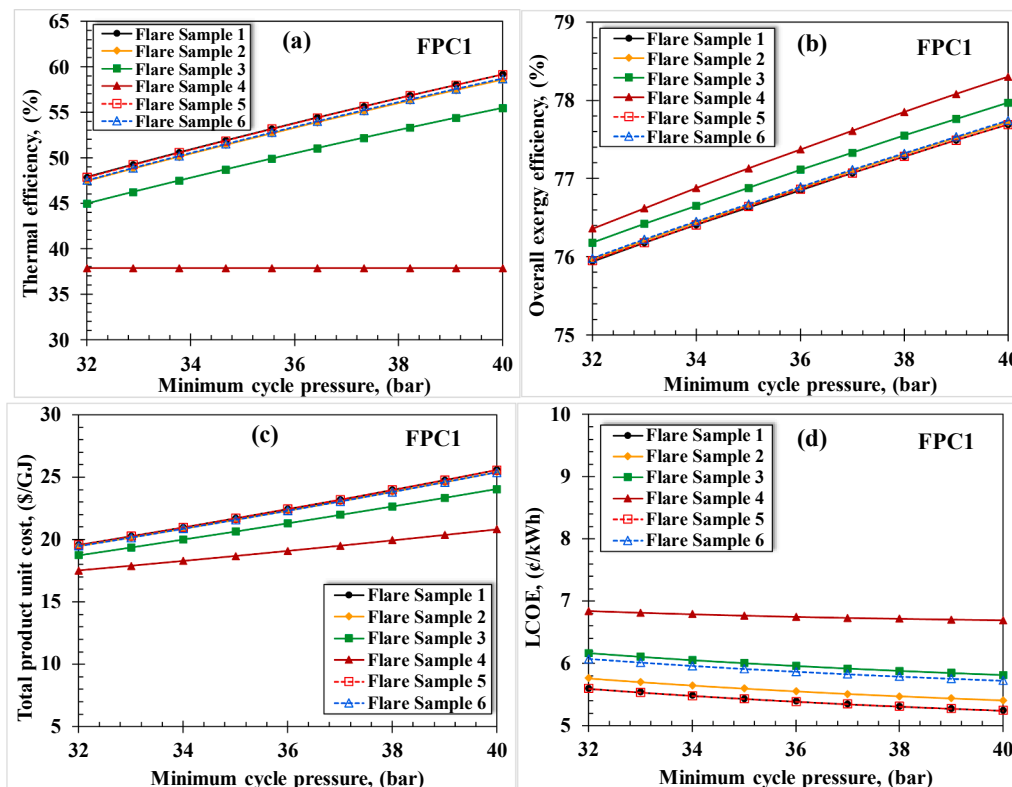

Fig. 7. Effect of the minimum cycle pressure on the (a) thermal efficiency, (b) exergy efficiency, (c) total product unit cost, and (d) LCOE of FPC1.
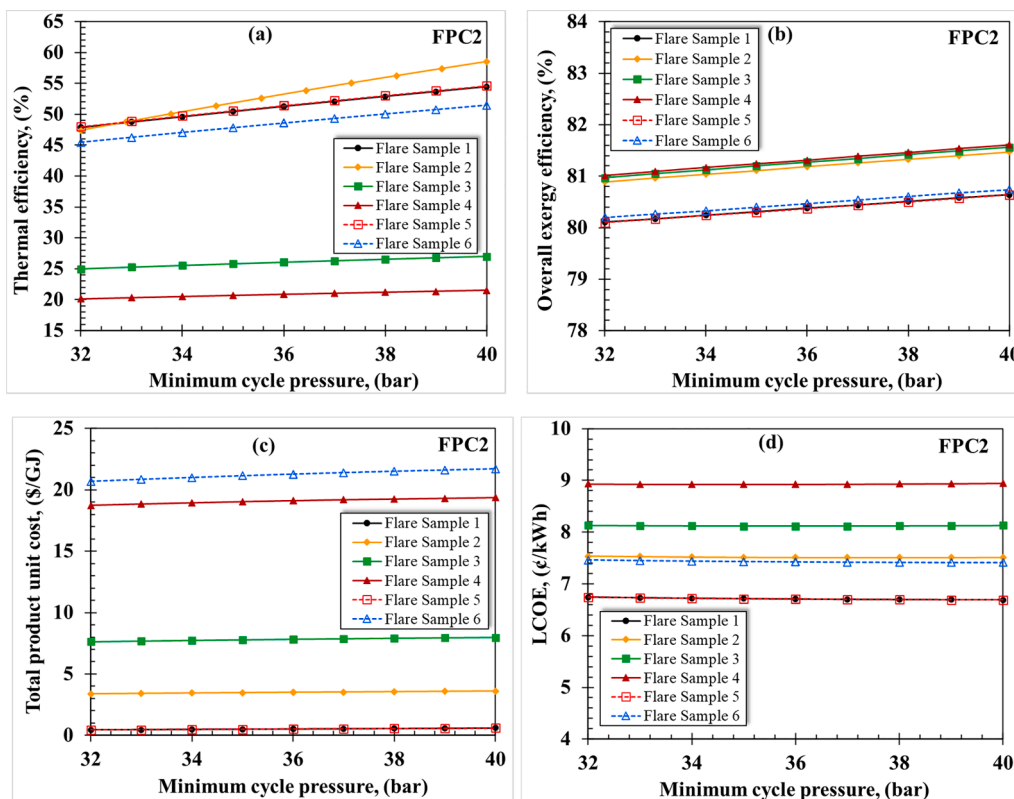
Fig. 8. Effect of the minimum cycle pressure on the (a) thermal efficiency, (b) exergy efficiency, (c) total product unit cost, and (d) LCOE of FPC2.
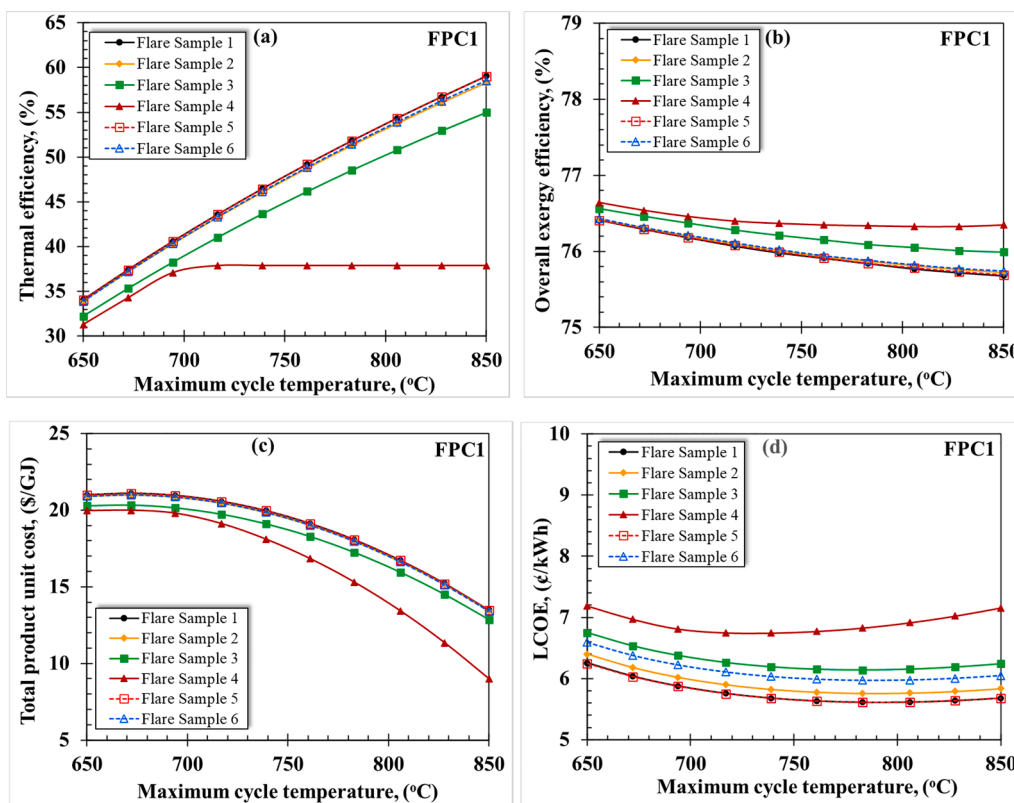

Fig. 9. Effect of the maximum cycle temperature on the (a) thermal efficiency, (b) exergy efficiency, (c) total product unit cost, and (d) LCOE of FPC1.
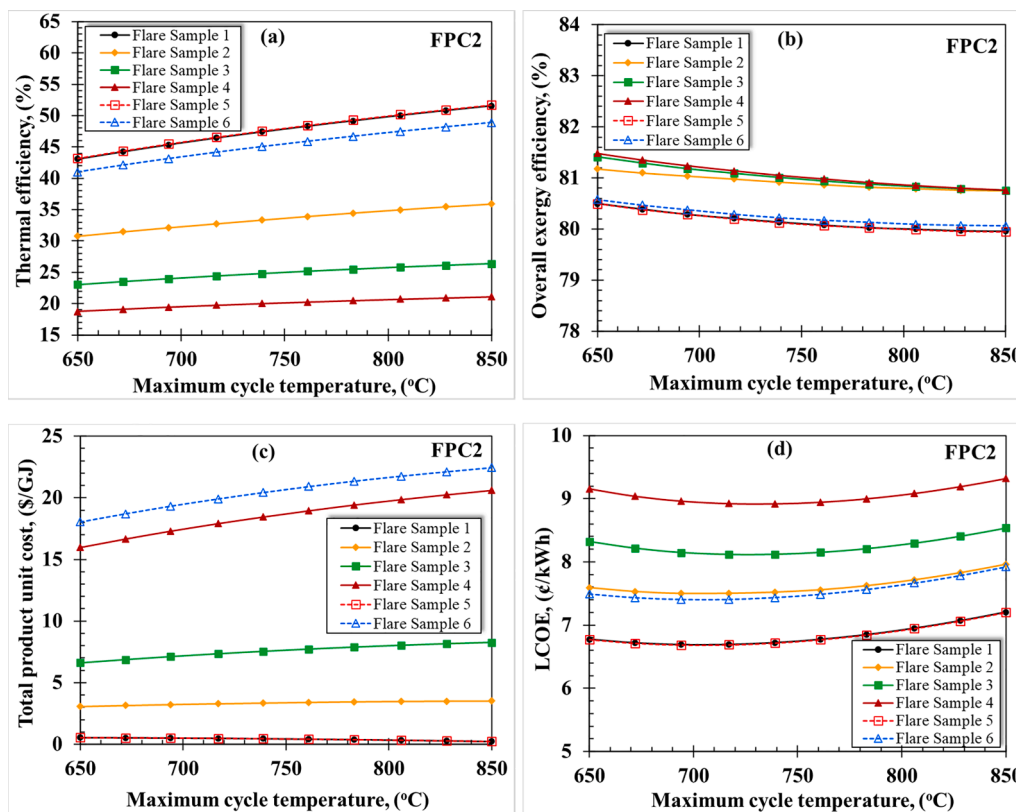
Fig. 10. Effect of the maximum cycle temperature on the (a) thermal efficiency, (b) exergy efficiency, (c) total product unit cost, and (d) LCOE of FPC2.
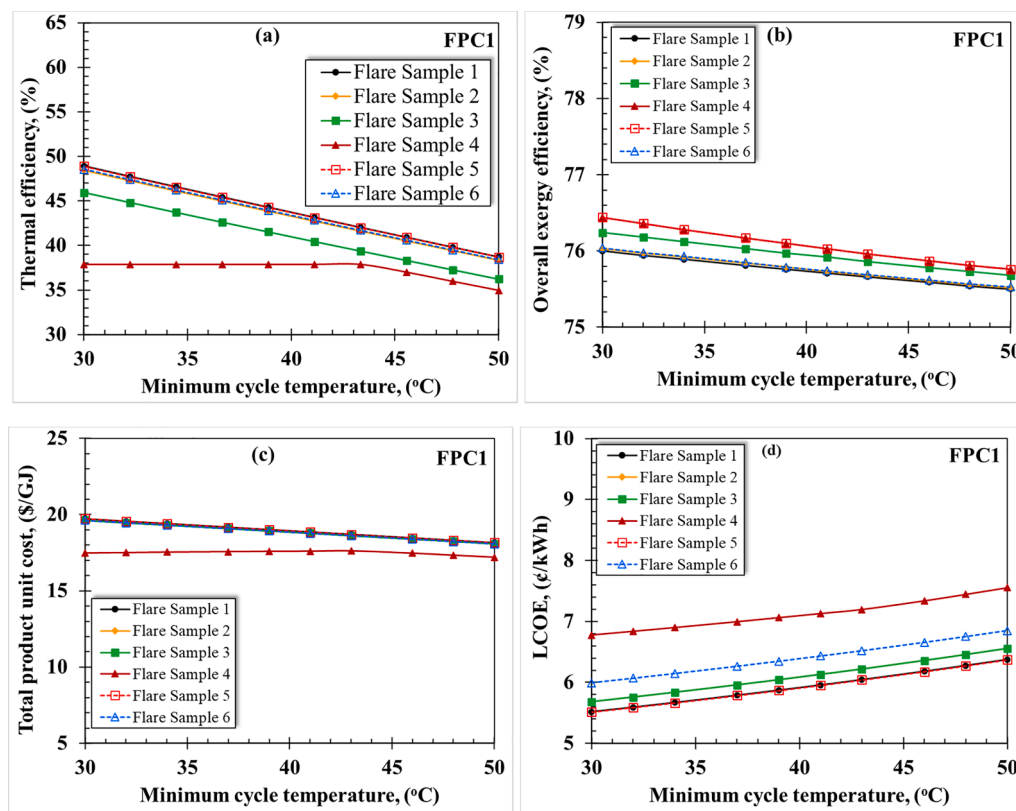

Fig. 11. Effect of the minimum cycle temperature on the (a) thermal efficiency, (b) exergy efficiency, (c) total product unit cost, and (d) LCOE of FPC1.

the turbines and recuperators.

The effect of T_{max} on the performance of FPC2 is similar to that of FPC1 (Fig. 10) except for the increase of $c_{p,total}$ with T_{max}. This returns to that the fuel exergy increases at higher rate than the rate of product exergy decrease for the cycle components. Moreover, the addition of the reheater and Turb. 2 in FPC2 further increase the capital and operational costs of the cycle which yields higher $c_{p,total}$. This also makes the LCOE in FPC2 (at power capacity of 50 MW) higher than in FPC1 by 22% (for sample 4) to 33% (for sample 5).

4.1.4. Effect of the minimum cycle temperature, T_{min}

Fig. 11 illustrates the effect of T_{min} of FPC1 on the thermal efficiency (Fig. 11 (a)), overall exergy efficiency (Fig. 11(b)), total product unit cost (Fig. 11 (c)), and on the LCOE (Fig. 11(d)). The η_{th} decreases with the increase of T_{min} as the compression power consumed by Comp.3 and Pump 1 significantly increases. The increase of T_{min} from 32 °C to 50 °C reduces the η_{th} by 10.15% for all flare samples except 4. The η_{th} of sample 4 remains constant up to T_{min} of 37.87 °C at which higher T_{min} dictates additional natural gas to be mixed and burned with the flare flow of sample 4, thus reduces η_{th}. While the increase of T_{min} improves the exergy efficiency of the DOC and the compressors, it significantly increases the exergy destruction of the HTR, LTR, PC, and IC. Therefore, the $\varepsilon_{overall}$ of the cycle decreases with the increase of T_{min}, Fig. 11(b). The $c_{p,total}$ slightly decreases with the increase of T_{min} since the decrease rate of the product exergies is much lower than the decrease rate of the fuel exergies of the heat exchanger components of the cycle, Fig. 11(c). Furthermore, the increase of T_{min} considerably increases the LCOE as the capital and operational costs of the compressors, recuperators, and the coolers of the cycle increase too, Fig. 11(d).

The performance of FPC2 is affected by the increase of T_{min} in a similar way for FPC1 (see Fig. 12). This since the variation of T_{min} affects the compression power of Comp. 3 and Pump 1 and the cooling loads of the PC and IC components which are common parts in both cycles.

However, FPC2 is less sensitive for the increase of T_{min} than FPC1. For instance, the thermal efficiency of FPC1 decreases by 20.9% as T_{min} increases from 30 °C to 50 °C while decrease by 12% in FPC2. This returns that the higher T_{min} increases the level of temperature in the high pressure side which has minimizing the heating load of the reheater.

4.1.5. Effect of the flare composition and specifications

This section focuses on the performance compassion between the investigated samples at the design point conditions. Fig. 13 compares the thermal efficiency (Fig. 13(a)), amount of consumed natural gas ($\dot{m}_{NG}$, Fig. 13 (b)), and the LCOE (Fig. 13(c)) of the six flare samples at three T_{max} temperatures for FPC1. Higher η_{th} is obtained at higher T_{max} for all samples except 4. Also, it can be noted that sample 4 consumes no natural gas at T_{max} of 750 °C and 850 °C. However, the low heating value of sample 4 compared to that of the natural gas makes the η_{th} of sample 4 much smaller than of the other samples. Consequently, the LCOE of sample 4 is the highest among the other samples. Furthermore, sweet samples (1 and 5) have the highest efficiency and the lowest LCOE compared to the other samples. Moreover, the LCOE at T_{max} of 750 °C is lower than at T_{max} of 650 °C or T_{max} of 850 °C, which implies that an optimization analysis must be performed to determine the optimum operating conditions for each configuration. These results disagree with the results of the indirect combustion of the flare gases to drive simple and combined gas power cycles published by Khalili-Garakani [23]. In [23], sample 4 shows superior performance since it has the maximum flow rate and maximum heat input for the bottoming cycle which enables it to produce the largest power capacity over the other samples. However, the indirect combustion of the flare gases is less efficient than the direct combustion as proposed in the present cycles (FPC1 and FPC2). Therefore, in FPC1, the LCOE for all samples is lower than reported in [23] for all samples. The opposite is true for the FPC2 (Fig. 14) where the indirect approach may be more efficient than the direct method. Therefore, the investigation of utilizing the flare gases to drive the sCO$_2$ closed power cycle with indirect-combustion is recommended
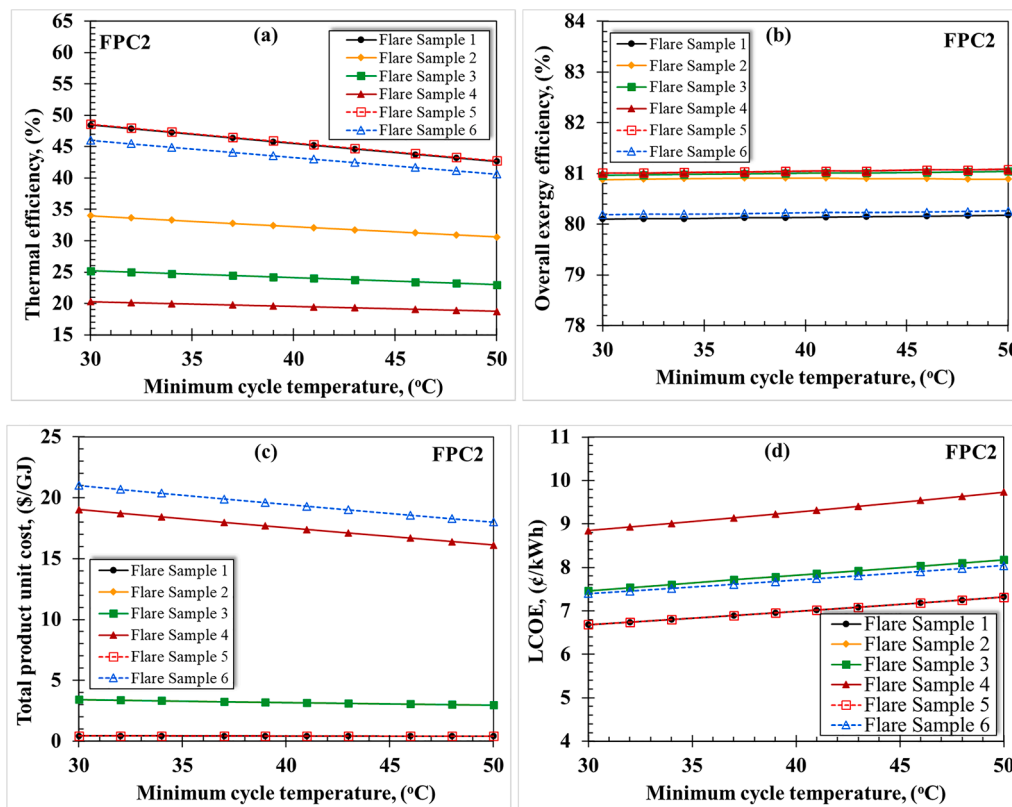

Fig. 12. Effect of the minimum cycle temperature on the (a) thermal efficiency, (b) exergy efficiency, (c) total product unit cost, and (d) LCOE of FPC2.
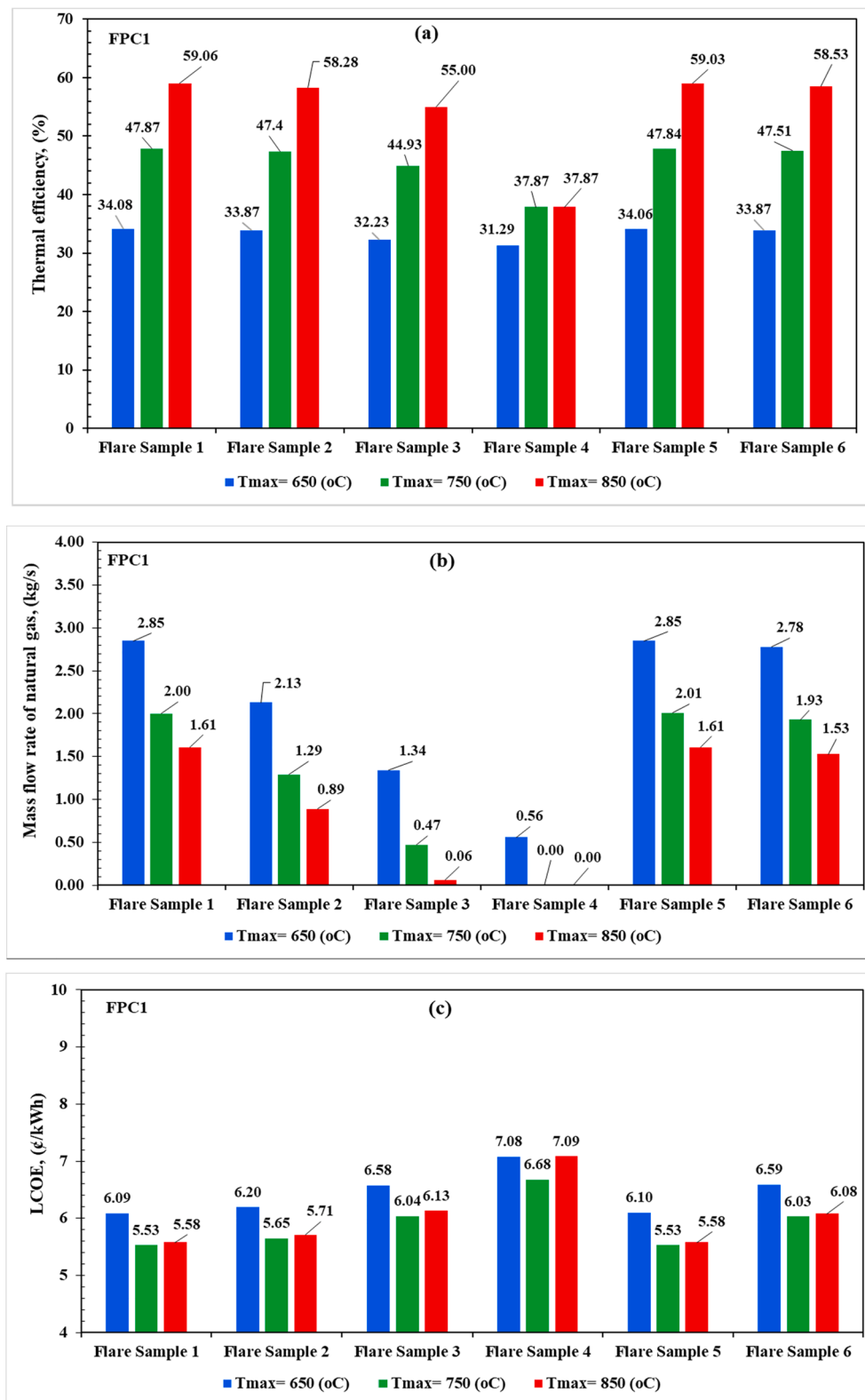
Fig. 13. Comparison of the sample performances in terms of (a) thermal efficiency, (b) flow rate of the natural gas, and (c) LCOE of FPC1.

for future work.

4.1.6. Comparison between the proposed configurations

In this section, a detailed comparison between FPC1 and FPC2 at two different capacities (50 MW and 100 MW) is presented in terms of several important parameters as shown in Table 6. The comparison was

conducted using sample 4 and sample 5 which have the lowest and the highest η_{th} among the other samples, respectively. It can be noted that at a net output power of 100 MW, η_{th} of sample 5 in FPC2 has higher η_{th} and lower LCOE than in FPC1 at the same conditions. This refers to that the reheating configurations of FPC2 can achieve competitive or superior performance compared to FPC1 at larger power cycle capacities (larger
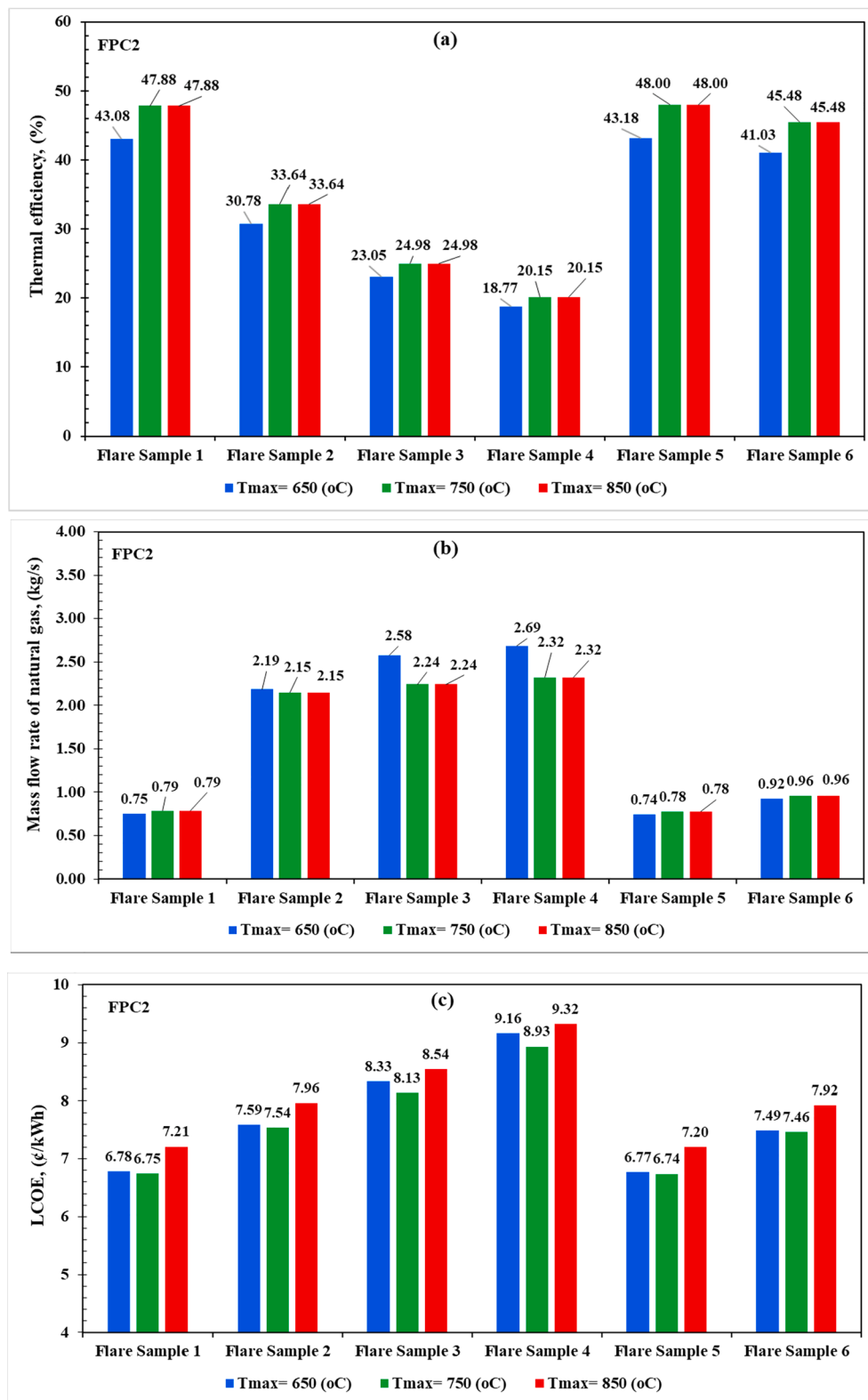
Fig. 14. Comparison of the sample performances in terms of (a) thermal efficiency, (b) flow rate of the natural gas, and (c) LCOE of FPC2.

than 100 MW). Furthermore, sample 4 has higher $\varepsilon_{overall}$ than sample 5, but the lower capital cost and the higher efficiency of sample 5 make its $c_{p,total}$ dramatically lower than of sample 4. Moreover, a minimum LCOE of 4.68¢/kWh is achieved by sample 5 in FPC1 at a power capacity of 100 MW.

Regarding the amount of the exported sCO_2, sample 4 exports a

maximum of 42.2 kg-sCO_2/s and a minimum of 4.8 kg-sCO_2/s in FPC2 at a power capacity of 100 MW. This means that at least 0.13–1.13 Mt sCO_2 can be captured per year. On the other hand, utilizing the flare gases to generate power by indirect combustion configurations increases the amount of CO_2 emissions to the ambient air. Therefore, the proposed configurations are considered promising solutions as they are able to

Table 6
Comparison between FPC1 and FPC2 at the design point conditions (Case 1).

| Item	FPC1				FPC2			
	50 MW		100 MW		50 MW		100 MW	
	Sample 4	Sample 5	Sample 4	Sample 5	Sample 4	Sample 5	Sample 4	Sample 5
η_{th}, (%)	37.87	47.84	45.70	48.02	20.15	48.11	28.35	49.37
$\varepsilon_{overall}$, (%)	76.35	75.95	76.11	75.93	81.01	80.29	80.94	80.24
$c_{p,total}$, ($/GJ)	17.55	19.57	16.69	17.28	18.72	0.44	20.89	0.40
LCOE, (¢/kWh)	6.69	5.53	5.23	4.68	8.93	6.75	7.00	5.70
Z_{total},(M$)	302.00	261.20	465.40	427.10	303.60	236.00	468.80	384.20
$\dot{Q}_{htr} + \dot{Q}_{ltr}$, (MW)	156.18	134.87	286.33	268.47	215.94	160.20	388.89	316.77
$\dot{Q}_{pc} + \dot{Q}_{ic}$, (MW)	160.11	138.63	293.99	275.97	136.82	101.76	246.33	201.25
$\dot{W}_{comp}$, (MW)	143.80	117.36	255.31	233.14	117.87	72.31	199.77	141.71
$\dot{m}_{NG}$, (kg/s)	0.00	2.01	1.74	4.08	2.32	0.78	4.41	1.40
$\dot{m}_{O_2}$, (kg/s)	15.64	8.73	22.58	17.03	24.93	3.82	33.29	6.30
$\dot{m}_{rCO_2,exp.}$, (kg/s)	12.76	6.02	17.53	11.73	31.80	4.80	42.20	7.90
$\dot{m}_{rCO_2}$, (kg/s)	574.20	502.30	1061.00	1000.00	495.10	372.00	890.50	736.30
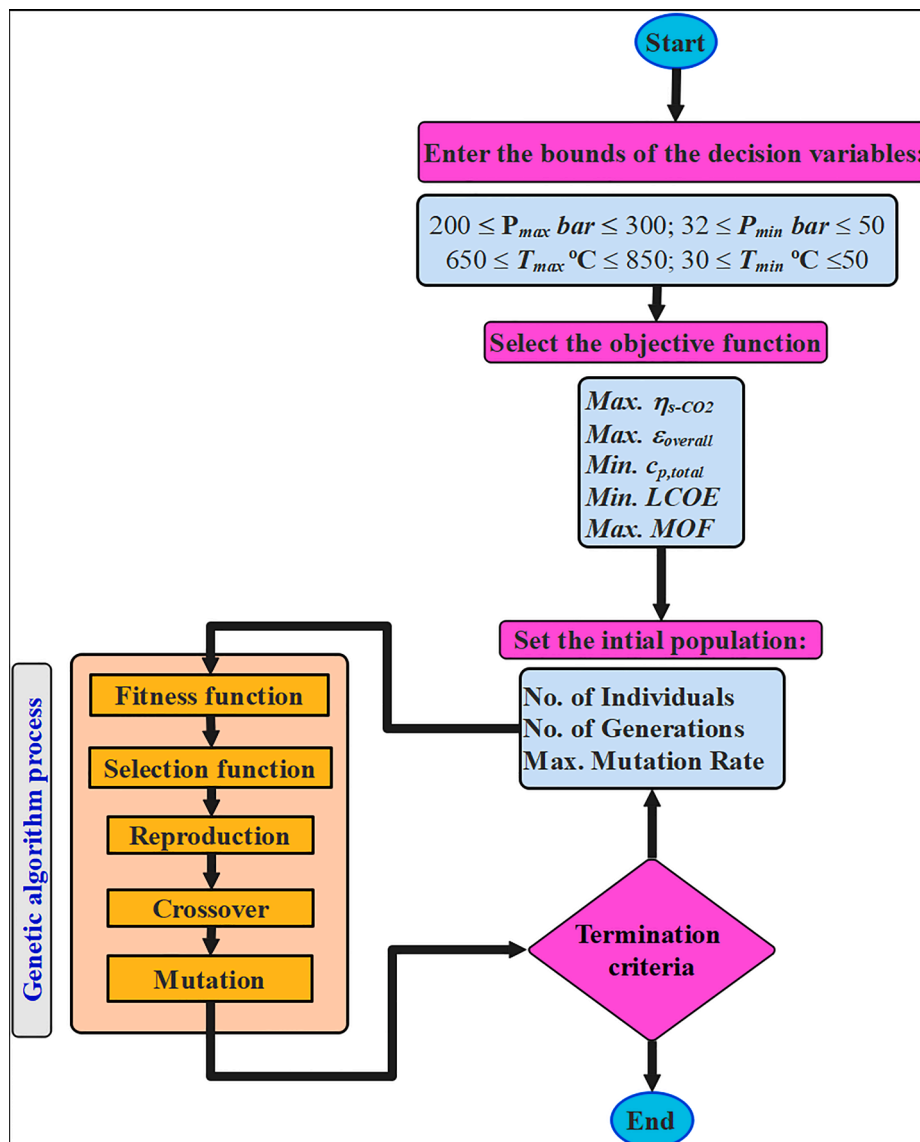
Fig. 15. Flow chart of optimization procedures.

utilize flare gases with various specifications with almost zero emissions to the atmosphere. Furthermore, direct combustion yields higher thermal efficiencies and lower LCOE if the cycle capacity and configuration are selected properly.

4.2. Optimization analysis

In this section, the optimized operating conditions for FPC1 and FPC2 are determined by performing single and multi-objective optimization analyses.

4.2.1. Optimization method

As discussed above, there are considerable differences between the optimal operating conditions of each configuration. Therefore, an optimization analysis is important for the key decision variables that yield high energetic and exergetic efficiencies and low product unit cost and LCOE. For this purpose, the genetic algorithm is used for single- and multi-objective optimization analysis of each cycle configuration following the procedures shown in Fig. 15. For the single-objective function (SOF) optimization analysis, the objective functions are: maximizing the thermal efficiency (*Max. η_{th}*), maximizing the overall exergy efficiency (*Max. $\varepsilon_{overall}$*), minimizing the total product unit cost (*Min. $c_{p,total}$*), and minimizing the LCOE (*Min. LCOE*). For the multi-objective function (MOF) optimization analysis, the objective function is defined by assigning a weighting coefficient for each objective functions [54] as follows:

$$Max.MOF = w_1 \times \eta_{th} + w_2 \times \varepsilon_{overall} + w_3 \times \left(1 - \frac{c_{p,total}}{C_{unit,f}}\right) + w_4 \times \left(1 - \frac{LCOE}{C_{fuel}}\right) \quad (31)$$

where w_1, w_2, w_3, and w_4 are the weighting coefficients for η_{th}, $\varepsilon_{overall}$, $c_{p,total}$, and LCOE, respectively. $c_{unit,f}$, and c_{fuel} are the unit fuel cost and the fuel cost which are 26.64 \$/GJ and 12¢/kWhe, respectively [54]. Considering that the four objective functions have the same importance, the weighting coefficients are assumed to be the same ($w_1 = w_2 = w_3 = w_4 = 1/4$) [49]. The results for the single-objective and multi-objective optimization analysis are provided for the following ranges of the decision variables:

$200 \leq P_{max}$ (bar) ≤ 300
$32 \leq P_{min}$ (bar) ≤ 50
$650 \leq T_{max}$ (°C) ≤ 850
$30 \leq T_{min}$ (°C) ≤ 50

4.2.2. Optimization results

From Table 7, it can be noted that the optimized values of the operating conditions differ significantly based on the used optimization function. For example, for sample 4 in FPC1, the optimized value of T_{max} is 850 °C for a maximum η_{th}, and 730 °C for a minimum LCOE. The minimum LCOE is achieved by the SOF (*Min. LCOE*) where the optimized conditions tend towards P_{max} of 300 bar, P_{min} of 40 bar, T_{max} of 730 °C, and T_{min} of 32 °C. In contrast, the results of the MOF tend toward P_{max} of 200 bar, P_{min} of 40 bar, T_{max} of 850 °C, and T_{min} of 32 °C. The results of the MOF may be more appropriate from safety and feasible design points of view. However, the results of the SOF (*Min. LCOE*) are more preferred from economic point of view. The minimum LCOE of FPC1 and FPC2 are 5.02¢/kWh and 5.96¢/kWh, respectively. These costs are achieved by sample 5 at T_{max} of 731 °C in FPC1 and 671 °C in FPC2 (with P_{max} of 300 bar, P_{min} of 40 bar, and T_{min} of 32 °C).

Also, from Table 7, it can be noted that the minimum LCOE is not

Table 8
Comparison between FPC1 and FPC2 at the design point conditions (Case 1).

Item	Heidari et al. [22]	Nezhadfard et al. [23]	Dwiyantoro et al. [80]	Present study	
				FPC1	FPC2
η_{th}, (%)	51.5	–	47.6	58.30	60.27
$\varepsilon_{overall}$, (%)	45.4	–	23.0	79.32	78.32
LCOE, (¢/kWh)	–	10.07	–	6.18	6.57
Flare flow rate, (kg/s)	0.32	0.19	0.20	0.19	0.19
Flare Heating Value, (kJ/kg)	31555	21890	41460	21890	21890
$\dot{W}_{net}$, (MW)	33.25	21.00	40.95	50	50
Capital cost (M \$)	24.30	51.56	–	261.20	236.00
Structure of the power block	Brayton cycle + steam Rankine cycle	Brayton cycle + steam Rankine cycle	Brayton cycle + steam Rankine cycle	DOC-sCO₂ power cycle	DOC-sCO₂ power cycle

Table 7
Results of the optimization analyses at an output capacity of 50 MW.

Cycle	Sample	Opt. function	Decision variables				Optimized results			
			P_{max} [bar]	P_{min} [bar]	T_{max} [°C]	T_{min} [°C]	η_{th} [%]	$\varepsilon_{overall}$ [%]	$c_{p,total}$ [\$/GJ]	LCOE [¢/kWh]
FPC1	Sample 4	*Max.η_{th}*	300	40	850	32	37.87	76.44	12.79	6.93
		Max. $\varepsilon_{overall}$	201	40	656	32	36.59	79.92	24.33	7.41
		Min. $c_{p,total}$	283	32	850	46	37.35	75.11	9.73	7.12
		Min. LCOE	296	40	730	33	37.87	77.25	21.94	6.10
		Max. MOF	200	40	697	32	37.87	79.84	23.54	7.34
	Sample 5	*Max.η_{th}*	201	39	850	32	58.28	79.19	18.10	6.19
		Max. $\varepsilon_{overall}$	200	40	650	32	39.69	79.72	26.01	6.35
		Min. $c_{p,total}$	298	32	850	45	41.92	74.50	10.09	5.88
		Min. LCOE	300	40	736	32	45.10	76.77	24.19	5.02
		Max. MOF	201	40	845	32	58.30	79.32	18.87	6.18
FPC2	Sample 4	*Max.η_{th}*	297	40	849	32	22.78	79.62	22.39	8.66
		Max. $\varepsilon_{overall}$	200	40	650	32	17.56	84.31	12.61	11.69
		Min. $c_{p,total}$	200	32	650	50	15.32	83.62	11.26	12.04
		Min. LCOE	300	34	731	32	21.23	79.62	20.05	8.21
		Max. MOF	200	39	835	32	20.94	83.98	17.95	10.73
	Sample 5	*Max.η_{th}*	300	40	849	32	61.38	78.66	0.38	6.51
		Max. $\varepsilon_{overall}$	200	40	850	32	47.43	83.75	0.37	9.09
		Min. $c_{p,total}$	230	32	847	50	45.40	81.19	0.22	8.10
		Min. LCOE	300	40	671	33	56.66	79.22	0.71	5.96
		Max. MOF	295	39	849	32	60.27	78.76	0.36	6.57

obtained at the maximum η_{th}. For instance, sample 5 (in FPC1) has a LCOE of 6.19¢/kWh with a η_{th} of 58.28% at a T_{max} of 850 °C. However, the same sample has a LCOE of 5.05¢/kWh with a η_{th} of 45.10% at T_{max} of 736 °C. This is explained by that T_{max} significantly increases the capital cost of the cycle, which dominates the LCOE more than the improvement achieved in the thermal efficiency.

Table 8 shows a comparison of the multi-optimized results of the present proposed cycles (FPC1 and FPC2) with other power systems that utilize flare gases for power generation [22,23,80]. These systems utilize combined power cycle block (Brayton cycle integrated with steam Rankine cycle) with using flare gases as a fuel source for the Brayton cycle combustor. It is clear that the DOC-sCO2 power cycle is more efficient than the combined cycle by an average of 9.7%. Although the capital cost of the DOC-sCO2 power block is much higher than of the combined block, the LCOE of the DOC is about 34.8% to 38.6% lower than the combined cycles. This is because the higher energy efficiency of the DOC-sCO2 system with higher power capacity than those reported for the combined power cycles.

5. Conclusions

This study investigates the advantages of integrating direct oxy-combustion (DOC) technology with two innovative flared-intercooled sCO2 power cycles that utilize flare gases and natural gas as fuel. In the first flared power cycle (FPC1), the flare gases are mixed with the natural gas before being combusted in the DOC. While in the second cycle (FPC2), the flare gases are used to perform a reheating process for the exhaust flow of the primary heater (DOC) after being partially expanded in a high-pressure turbine. These cycles are promising configurations to realize the goal of "no flaring-no emissions" that yields several economic and environmental benefits. Thorough energetic, exergetic, exergoeconomic, LCOE, and optimization analyses have been conducted for each configuration over practical ranges of operating conditions. Furthermore, the simulation results were investigated for six flare gas samples that differ significantly in their composition and specifications. To ensure almost zero emissions, the SOx and NOx resulted from the flare combustions are considered to be removed and the cost of the removing units was included in the analysis. The main conclusions of this study are summarized as follows:

- At a power capacity of 50 MW, FPC1 has higher η_{th} and lower LCOE than FPC2 for all investigated samples. However, FPC2 has higher η_{th} than FPC1 at a power capacity of 100 MW, since reheated configurations are more efficient at larger capacities.
- Sweet flare gas samples (1 and 5) show superior performance and lower LCOE due to their low flow rate (so they consume additional natural gas, which is more efficient than the flare gas) and these samples have zero cost for removing SOx and NOx.
- By the SOF (*Min. LCOE*), a minimum LCOE of 5.02¢/kWh is achieved by sample 5 in FPC1 at T_{max} of 731 °C, P_{max} of 300 bar, P_{min} of 40 bar, T_{min} of 32 °C, and $\dot{W}_{net}$ of 50 MW.
- Sample 4 exports a maximum of 42.2 kg-sCO2/s and a minimum of 4.8 kg-sCO2/s in FPC2 at a power capacity of 100 MW, which is equivalent to 0.13–1.13 Mt of sCO2/year.
- At the optimized conditions, FPC1 and FPC2 show superior energetic and economic performances compared to indirect-combustion power cycles that utilize flare gas as fuel. However, indirect combustion of the flare gases may perform better than FPC2 at low capacities and therefore recommended for future work.

CRediT authorship contribution statement

Ahmad K. Sleiti: Conceptualization, Investigation, Writing - original draft, Writing - review & editing, Resources, Formal analysis, Project administration, Funding acquisition, Supervision. **Wahib A. Al-** **Ammari:** Conceptualization, Writing - original draft, Investigation, Software, Data curation, Validation, Formal analysis. **Khaled M. Aboueata:** Writing - review & editing, Visualization.

Declaration of Competing Interest

The authors declare that they have no known competing financial interests or personal relationships that could have appeared to influence the work reported in this paper.

Appendix A. Supplementary data

Supplementary data to this article can be found online at https://doi.org/10.1016/j.fuel.2021.121808.

References

[1] Global Gas Flaring Reduction Partnership. Global Gas Flaring Tracker Report. 2020.
[2] Mansoor R, Tahir M. Recent developments in natural gas flaring reduction and reformation to energy-efficient fuels: a review. Energy Fuels 2021. https://doi.org/10.1021/acs.energyfuels.0c04269.
[3] Trivanovic U, Sipkens TA, Kazemimanesh M, Baldelli A, Jefferson AM, Conrad BM, et al. Morphology and size of soot from gas flares as a function of fuel and water addition. Fuel 2020;279:118478. https://doi.org/10.1016/j.fuel.2020.118478.
[4] Beigiparast S, Tahouni N, Abbasi M, Panjeshahi MH. Flare gas reduction in an olefin plant under different start-up procedures. Energy 2021;214:118927. https://doi.org/10.1016/j.energy.2020.118927.
[5] Zamani M, Abbasi-Atibeh E, Mobaseri S, Ahsan H, Ahsan A, Olfert JS, et al. An experimental study on the carbon conversion efficiency and emission indices of air and steam co-flow diffusion jet flames. Fuel 2021;287:119534. https://doi.org/10.1016/j.fuel.2020.119534.
[6] Abdulrahman AO, Huisingh D, Hafkamp W. Sustainability improvements in Egypt's oil & gas industry by implementation of flare gas recovery. J Clean Prod 2015;98:116–22. https://doi.org/10.1016/j.jclepro.2014.11.086.
[7] Khalili-Garakani A, Iravaninia M, Nezhadfard M. A review on the potentials of flare gas recovery applications in Iran. J Clean Prod 2021;279:123345. https://doi.org/10.1016/j.jclepro.2020.123345.
[8] Ojijiagwo E, Oduoza CF, Emekwuru N. Economics of gas to wire technology applied in gas flare management. Eng Sci Technol an Int J 2016;19:2109–18. https://doi.org/10.1016/j.jestch.2016.09.012.
[9] Bauer M, Engineering T, Köck M, Jörg K, Ramakrishnan C, Engineering T, et al. Flare-gas recovery in Tunisia — from liability to value. Oil Gas Facil 2012;1:44–51. https://doi.org/10.2118/155946-PA.
[10] Emam EA. GAS flaring in industry: an overview. Pet Coal 2015;57:532–55.
[11] Woldeyohannes AD, Majid MAA. Simulation model for natural gas transmission pipeline network system. Simul Model Pract Theory 2011;19:196–212. https://doi.org/10.1016/j.simpat.2010.06.006.
[12] Nwaoha C, Wood DA. A review of the utilization and monetization of Nigeria's natural gas resources: current realities. J Nat Gas Sci Eng 2014;18:412–32. https://doi.org/10.1016/j.jngse.2014.03.019.
[13] Johnson MR, Coderre AR. Opportunities for CO 2 equivalent emissions reductions via flare and vent mitigation: a case study for Alberta, Canada. Int J Greenh Gas Control 2012;8:121–31. https://doi.org/10.1016/j.ijggc.2012.02.004.
[14] Hajizadeh A, Mohamadi-Baghmolaei M, Azin R, Osfouri S, Heydari I. Technical and economic evaluation of flare gas recovery in a giant gas refinery. Chem Eng Res Des 2018;131:506–19. https://doi.org/10.1016/j.cherd.2017.11.026.
[15] Yazdani E, Asadi J, Dehaghani YH, Kazempoor P. Flare gas recovery by liquid ring compressors-system design and simulation. J Nat Gas Sci Eng 2020;84:103627. https://doi.org/10.1016/j.jngse.2020.103627.
[16] Odumugbo CA. Natural gas utilisation in Nigeria: challenges and opportunities. J Nat Gas Sci Eng 2010;2:310–6. https://doi.org/10.1016/j.jngse.2010.08.004.
[17] Rahimpour MR, Jokar SM. Feasibility of flare gas reformation to practical energy in Farashband gas refinery: No gas flaring. J Hazard Mater 2012;209–210:204–17. https://doi.org/10.1016/j.jhazmat.2012.01.017.

[18] Rahimpour MR, Jamshidnejad Z, Jokar SM, Karimi G, Ghorbani A, Mohammadi AH. A comparative study of three different methods for flare gas recovery of Asalooye Gas Refinery. J Nat Gas Sci Eng 2012;4:17–28. https://doi.org/10.1016/j.jngse.2011.10.001.

[19] Iora P, Bombarda P, Gómez Aláez SL, Invernizzi C, Rajabloo T, Silva P. Flare gas reduction through electricity production. Energy Sources, Part A Recover Util Environ Eff 2016;38:3116–24. https://doi.org/10.1080/15567036.2015.1129471.

[20] Saidi M, Siavashi F, Rahimpour MR. Application of solid oxide fuel cell for flare gas recovery as a new approach; a case study for Asalouyeh gas processing plant, Iran. J Nat Gas Sci Eng 2014;17:13–25. https://doi.org/10.1016/j.jngse.2013.12.005.

[21] Shayan M, Pirouzfar V, Sakhaeinia H. Technological and economical analysis of flare recovery methods, and comparison of different steam and power generation systems. J Therm Anal Calorim 2020;139:2399–411. https://doi.org/10.1007/s10973-019-08429-9.

[22] Heidari M, Ataei A, Rahdar MH. Development and analysis of two novel methods for power generation from flare gas. Appl Therm Eng 2016;104:687–96. https://doi.org/10.1016/j.applthermaleng.2016.05.099.

[23] Nezhadfard M, Khalili-Garakani A. Power generation as a useful option for flare gas recovery: enviro-economic evaluation of different scenarios. Energy 2020;204:117940. https://doi.org/10.1016/j.energy.2020.117940.

[24] Senior CL, Morris W, Lewandowski TA. Emissions and risks associated with oxyfuel combustion: State of the science and critical data gaps. J Air Waste Manag Assoc 2013;63:832–43. https://doi.org/10.1080/10962247.2013.791892.

[25] Schluckner C, Gaber C, Landfahrer M, Demuth M, Hochenauer C. Fast and accurate CFD-model for NOx emission prediction during oxy-fuel combustion of natural gas using detailed chemical kinetics. Fuel 2020;264:116841. https://doi.org/10.1016/j.fuel.2019.116841.

[26] Yadav S, Mondal SS. Numerical investigation of 660 MW pulverized coal-fired supercritical power plant retrofitted to oxy-coal combustion. Int J Greenh Gas Control 2021;105:103227. https://doi.org/10.1016/j.ijggc.2020.103227.

[27] Ferrari N, Mancuso L, Davison J, Chiesa P, Martelli E, Romano MC. Oxy-turbine for power plant with CO2 capture. Energy Procedia 2017;114:471–80. https://doi.org/10.1016/j.egypro.2017.03.1189.

[28] Zhang Yu, Vangaever S, Theis G, Henneke M, Heynderickx GJ, Van Geem KM. Feasibility of biogas and oxy-fuel combustion in steam cracking furnaces: Experimental and computational study. Fuel 2021;304:121393. https://doi.org/10.1016/j.fuel.2021.121393.

[29] Abraham BM, Asbury JG, Lynch EP, Teotia APS. Coal-oxygen process provides CO2 for enhanced recovery. Oil Gas J 1982;80:68–70.

[30] Chan W, Lei X, Chang F, Li H. Thermodynamic analysis and optimization of Allam cycle with a reheating configuration. Energy Convers Manag 2020;224:113382. https://doi.org/10.1016/j.enconman.2020.113382.

[31] Zhao Y, Chi J, Zhang S, Xiao Y. Thermodynamic study of an improved MATIANT cycle with stream split and recompression. Appl Therm Eng 2017;125:452–69. https://doi.org/10.1016/j.applthermaleng.2017.05.023.

[32] González Álvarez JF, Alonso Fernández E. Oxy-combustion flow field study under power-generating and CO2-capturing Matiant cycle conditions and its influence on the turbine inlet conditions. Fuel 2021;303:121172. https://doi.org/10.1016/j.fuel.2021.121172.

[33] Jericha H, Sanz W, Göttlich E. Design concept for large output Graz Cycle gas turbines. J Eng Gas Turbines Power 2008;130:1–10. https://doi.org/10.1115/1.2747260.

[34] Bolland O, Mathieu P. Comparison of two CO2 removal options in combined cycle power plants. Energy Convers Manag 1998;39:1653–63. https://doi.org/10.1016/S0196-8904(98)00078-8.

[35] Allam RJ, Fetvedt JE, Forrest BA, Freed DA. The OXY-fuel, supercritical CO2 allam cycle: New cycle developments to produce even lower-cost electricity from fossil fuels without atmospheric emissions. Proc ASME Turbo Expo 2014;GT2014-269:1–9. https://doi.org/10.1115/GT2014-26952.

[36] Weiland NT, White CW. Techno-economic analysis of an integrated gasification direct-fired supercritical CO2 power cycle. Fuel 2018;212:613–25. https://doi.org/10.1016/j.fuel.2017.10.022.

[37] Crespi F, Gavagnin G, Sánchez D, Martínez GS. Supercritical carbon dioxide cycles for power generation: a review. Appl Energy 2017;195:152–83. https://doi.org/10.1016/j.apenergy.2017.02.048.

[38] Fernandes D, Wang S, Xu Q, Chen D. Dynamic simulations of the allam cycle power plant integrated with an air separation unit. Int J Chem Eng 2019;2019:325–40. https://doi.org/10.1155/2019/6035856.

[39] Allam RJ, Palmer MR, Brown GW, Fetvedt J, Freed D, Nomoto H, et al. High efficiency and low cost of electricity generation from fossil fuels while eliminating atmospheric emissions, including carbon dioxide. Energy Procedia 2013;37:1135–49. https://doi.org/10.1016/j.egypro.2013.05.211.

[40] Allam R, Martin S, Forrest B, Fetvedt J, Lu X, Freed D, et al. Demonstration of the allam cycle: an update on the development status of a high efficiency supercritical carbon dioxide power process employing full carbon capture. Energy Procedia 2017;114:5948–66. https://doi.org/10.1016/j.egypro.2017.03.1731.

[41] Chakroun NW, Ghoniem AF. High-efficiency low LCOE combined cycles for sour gas oxy-combustion with CO2 capture. Int J Greenh Gas Control 2015;41:1–11. https://doi.org/10.1016/j.ijggc.2015.06.025.

[42] Scaccabarozzi R, Gatti M, Martelli E. Thermodynamic analysis and numerical optimization of the NET Power oxy-combustion cycle. Appl Energy 2016;178:505–26. https://doi.org/10.1016/j.apenergy.2016.06.060.

[43] Rogalev A, Grigoriev E, Kindra V, Rogalev N. Thermodynamic optimization and equipment development for a high efficient fossil fuel power plant with zero emissions. J Clean Prod 2019;236:117592. https://doi.org/10.1016/j.jclepro.2019.07.067.

[44] Zhu Z, Chen Y, Wu J, Zhang S, Zheng S. A modified Allam cycle without compressors realizing efficient power generation with peak load shifting and CO2 capture. Energy 2019;174:478–87. https://doi.org/10.1016/j.energy.2019.01.165.

[45] Sleiti AK, Al-Ammari W, Ahmed S, Kapat J. Direct-fired oxy-combustion supercritical-CO2 power cycle with novel preheating configurations -thermodynamic and exergoeconomic analyses. Energy 2021;226:120441. https://doi.org/10.1016/j.energy.2021.120441.

[46] Sleiti AK, Al-Ammari WA. Energy and exergy analyses of novel supercritical CO2 Brayton cycles driven by direct oxy-fuel combustor. Fuel 2021;294:120557. https://doi.org/10.1016/j.fuel.2021.120557.

[47] Zhu Q. Innovative power generation systems using supercritical CO2 cycles. Clean Energy 2017. https://doi.org/10.1093/ce/zkx003.

[48] Ghaebi H, Parikhani T, Rostamzadeh H, Farhang B. Thermodynamic and thermoeconomic analysis and optimization of a novel combined cooling and power (CCP) cycle by integrating of ejector refrigeration and Kalina cycles. Energy 2017;139:262–76. https://doi.org/10.1016/j.energy.2017.07.154.

[49] Boyaghchi FA, Chavoshi M, Sabeti V. Optimization of a novel combined cooling, heating and power cycle driven by geothermal and solar energies using the water/CuO (copper oxide) nanofluid. Energy 2015;91:685–99. https://doi.org/10.1016/j.energy.2015.08.082.

[50] Rostamzadeh H, Ghaebi H, Parikhani T. Thermodynamic and thermoeconomic analysis of a novel combined cooling and power (CCP) cycle. Appl Therm Eng 2018;139:474–87. https://doi.org/10.1016/j.applthermaleng.2018.05.001.

[51] Akbari AD, Mahmoudi SMS. Thermoeconomic analysis & optimization of the combined supercritical CO2 (carbon dioxide) recompression Brayton/organic Rankine cycle. Energy 2014;78:501–12. https://doi.org/10.1016/j.energy.2014.10.037.

[52] Luo D, Huang D. Thermodynamic and exergoeconomic investigation of various SCO2 Brayton cycles for next generation nuclear reactors. Energy Convers Manag 2020;209:112649. https://doi.org/10.1016/j.enconman.2020.112649.

[53] Liu Z, Liu Z, Cao X, Luo T, Yang X. Advanced exergoeconomic evaluation on supercritical carbon dioxide recompression Brayton cycle. J Clean Prod 2020;256:120537. https://doi.org/10.1016/j.jclepro.2020.120537.

[54] Alharbi S, Elsayed ML, Chow LC. Exergoeconomic analysis and optimization of an integrated system of supercritical CO2 Brayton cycle and multi-effect desalination. Energy 2020;197:117225. https://doi.org/10.1016/j.energy.2020.117225.

[55] Fan G, Li H, Du Y, Zheng S, Chen K, Dai Y. Preliminary conceptual design and thermo-economic analysis of a combined cooling, heating and power system based on supercritical carbon dioxide cycle. Energy 2020;203:117842. https://doi.org/10.1016/j.energy.2020.117842.

[56] Zhang F, Liao G, E J, Chen J, Leng E, Sundén B. Thermodynamic and exergoeconomic analysis of a novel CO2 based combined cooling, heating and power system. Energy Convers Manag 2020;222:113251. https://doi.org/10.1016/j.enconman.2020.113251.

[57] Chen Y, Wang M, Liso V, Samsatli S, Samsatli NJ, Jing R, et al. Parametric analysis and optimization for exergoeconomic performance of a combined system based on solid oxide fuel cell-gas turbine and supercritical carbon dioxide Brayton cycle. Energy Convers Manag 2019;186:66–81. https://doi.org/10.1016/j.enconman.2019.02.036.

[58] Wu C, Wang S sen, Li J. Exergoeconomic analysis and optimization of a combined supercritical carbon dioxide recompression Brayton/organic flash cycle for nuclear power plants. Energy Convers Manag 2018;171:936–52. https://doi.org/10.1016/j.enconman.2018.06.041.

[59] Ruiz-Casanova E, Rubio-Maya C, Pacheco-Ibarra JJ, Ambriz-Díaz VM, Romero CE, Wang X. Thermodynamic analysis and optimization of supercritical carbon dioxide Brayton cycles for use with low-grade geothermal heat sources. Energy Convers Manag 2020;216:112978. https://doi.org/10.1016/j.enconman.2020.112978.

[60] Liu Y, Wang Y, Huang D. Supercritical CO2 Brayton cycle: a state-of-the-art review. Energy 2019;189:115900. https://doi.org/10.1016/j.energy.2019.115900.

[61] Wang X, Yablonsky GS, ur Rahman Z, Yang Z, Du P, Tan H, et al. Assessment of sulfur trioxide formation due to enhanced interaction of nitrogen oxides and sulfur oxides in pressurized oxy-combustion. Fuel 2021;290:119964. https://doi.org/10.1016/j.fuel.2020.119964.

[62] Yuan Z, Meng L, Gu X, Bai Y, Cui H, Jiang C. Prediction of NOx emissions for coal-fired power plants with stacked-generalization ensemble method. Fuel 2021;289:119748. https://doi.org/10.1016/j.fuel.2020.119748.

[63] Ximinis J, Massaguer A, Pujol T, Massaguer E. Nox emissions reduction analysis in a diesel Euro VI Heavy Duty vehicle using a thermoelectric generator and an exhaust heater. Fuel 2021;301:121029. https://doi.org/10.1016/j.fuel.2021.121029.

[64] Doctor R, Coleman C, Austell M. Transport of CO2. IPCC Spec. Rep. Carbon dioxide Capture Storage, 2005.

[65] Lu H, Ma X, Huang K, Fu L, Azimi M. Carbon dioxide transport via pipelines: a systematic review. J Clean Prod 2020;266:121994. https://doi.org/10.1016/j.jclepro.2020.121994.

[66] Onyebuchi VE, Kolios A, Hanak DP, Biliyok C, Manovic V. A systematic review of key challenges of CO2 transport via pipelines. Renew Sustain Energy Rev 2018;81:2563–83. https://doi.org/10.1016/j.rser.2017.06.064.

[67] Shublaq M, Sleiti AK. Experimental analysis of water evaporation losses in cooling towers using filters. Appl Therm Eng 2020;175:115418. https://doi.org/10.1016/j.applthermaleng.2020.115418.

[68] Thanganadar D, Asfand F, Patchigolla K. Thermal performance and economic analysis of supercritical Carbon Dioxide cycles in combined cycle power plant. Appl Energy 2019;255:113836. https://doi.org/10.1016/j.apenergy.2019.113836.

[69] Tozlu A, Abuşoğlu A, Özahi E. Thermoeconomic analysis and optimization of a Re-compression supercritical CO2 cycle using waste heat of Gaziantep Municipal Solid Waste Power Plant. Energy 2018;143:168–80. https://doi.org/10.1016/j.energy.2017.10.120.

[70] Noaman M, Saade G, Morosuk T, Tsatsaronis G. Exergoeconomic analysis applied to supercritical CO2 power systems. Energy 2019;183:756–65. https://doi.org/10.1016/j.energy.2019.06.161.

[71] Wright S, Scammell W. Economics. Fundam. Appl. Supercrit. Carbon Dioxide Based Power Cycles, 2017, p. 127–45. https://doi.org/10.1016/B978-0-08-100804-1.00006-2.

[72] Weiland NT, Lance BW, Pidaparti SR. SCO2 power cycle component cost correlations from DOE data spanning multiple scales and applications. Proc ASME Turbo Expo 2019;9:1–18. https://doi.org/10.1115/GT2019-90493.

[73] Zare V, Mahmoudi SMS, Yari M, Amidpour M. Thermoeconomic analysis and optimization of an ammonia-water power/cooling cogeneration cycle. Energy 2012;47:271–83. https://doi.org/10.1016/j.energy.2012.09.002.

[74] Sleiti AK, Al-Ammari WA, Al-Khawaja M. Integrated novel solar distillation and solar single-effect absorption systems. Desalination 2021;507:115032. https://doi.org/10.1016/j.desal.2021.115032.

[75] Ma Y, Morosuk T, Luo J, Liu M, Liu J. Superstructure design and optimization on supercritical carbon dioxide cycle for application in concentrated solar power plant. Energy Convers Manag 2020;206:112290. https://doi.org/10.1016/j.enconman.2019.112290.

[76] Mohammadi K, Ellingwood K, Powell K. A novel triple power cycle featuring a gas turbine cycle with supercritical carbon dioxide and organic Rankine cycles: Thermoeconomic analysis and optimization. Energy Convers Manag 2020;220:113123. https://doi.org/10.1016/j.enconman.2020.113123.

[77] Zhang N, Lior N, Liu M, Han W. COOLCEP (cool clean efficient power): A novel CO2-capturing oxy-fuel power system with LNG (liquefied natural gas) coldness energy utilization. Energy 2010;35:1200–10. https://doi.org/10.1016/j.energy.2009.04.002.

[78] Luo J, Emelogu O, Morosuk T, Tsatsaronis G. Exergy-based investigation of a coal-fired allam cycle. Energy 2021;218:119471. https://doi.org/10.1016/j.energy.2020.119471.

[79] Dyreby JJ, Klein SA, Nellis GF, Reindl DT. Modeling off-design and part-load performance of supercritical carbon dioxide power cycles. Proc ASME Turbo Expo 2013;8:1–7. https://doi.org/10.1115/GT2013-95824.

[80] Dwiyantoro BA, Saungweme FW. Analysis of an optimum method for power generation using flare gas from oil refinery plants. AIP Conf Proc 2019;2187. https://doi.org/10.1063/1.5138290.